



**HAL**  
open science

## Adaptive interface thickness based mobility-Phase-field method for incompressible fluids

Deewakar Sharma, Mathieu Coquerelle, Arnaud Erriguible, Sakir Amiroudine

► **To cite this version:**

Deewakar Sharma, Mathieu Coquerelle, Arnaud Erriguible, Sakir Amiroudine. Adaptive interface thickness based mobility-Phase-field method for incompressible fluids. *International Journal of Multiphase Flow*, 2021, 142, pp.103687. 10.1016/j.ijmultiphaseflow.2021.103687 . hal-03482879

**HAL Id: hal-03482879**

**<https://hal.science/hal-03482879>**

Submitted on 13 Jun 2023

**HAL** is a multi-disciplinary open access archive for the deposit and dissemination of scientific research documents, whether they are published or not. The documents may come from teaching and research institutions in France or abroad, or from public or private research centers.

L'archive ouverte pluridisciplinaire **HAL**, est destinée au dépôt et à la diffusion de documents scientifiques de niveau recherche, publiés ou non, émanant des établissements d'enseignement et de recherche français ou étrangers, des laboratoires publics ou privés.



Distributed under a Creative Commons Attribution - NonCommercial 4.0 International License

## Adaptive interface thickness based mobility - Phase-field method for incompressible fluids

Deewakar Sharma<sup>1</sup>, Mathieu Coquerelle<sup>2</sup>, Arnaud Erriguible<sup>2</sup> and Sakir Amiroudine<sup>1\*</sup>

<sup>1</sup> *University of Bordeaux, I2M CNRS, Talence, F-33400, France*

<sup>2</sup> *Bordeaux INP, University of Bordeaux, CNRS, Arts et Metiers Institute of Technology, INRAE, I2M Bordeaux, F-33600 Talence, France*

\*corresponding author

### Abstract

The ubiquity of two-phase systems has rendered them a subject of prime importance especially from numerical perspectives. Among several methods described in the literature, which are generally classified as sharp or diffuse interface methods, phase-field (diffuse interface) method has been at the paramount of several recent investigations owing to its several advantages, primarily to handle complex topological changes. Though several advancements have been made in the subject, one of the important challenges with this approach using Cahn-Hilliard equation lies in the determination of an appropriate value of mobility. Despite certain propositions in the literature in terms of non-dimensional numbers (Peclet and Cahn numbers), ambiguity in the velocity scale to be chosen for evaluating mobility poses a challenge for their **straightforward** extension to real systems. In addition it renders the system to be dependent on numerical parameters. In the current work, we address this problem using a new approach to calculate the mobility parameter in terms of local equilibrium interface thickness which in itself is evaluated from the phase-field. Consequently, this helps to make the model independent of numerical parameters making it more reliable. We test this approach for several canonical and complex cases, such as the rise of lighter bubble in a heavier medium, bubble coalescence, Rayleigh-Taylor instability. The results are compared with those in literature or obtained using level set method. An excellent agreement is observed illustrating the potential of this approach to make phase-field model more prominent.

**Key words:** Phase-field method, two-phase flow, Cahn-Hilliard equation, mobility, adaptive thickness.

## 1. Introduction

Several physical processes in industrial and scientific applications consist of more than two fluids or interacting phases such as in heat transfer systems, power systems, process engineering etc. and they are categorized as two-phase flow systems. Understanding the flow dynamics in these systems is of prime importance for their efficient design and utility. With limitations in experimental techniques, mathematical modelling provides an alternative pathway especially in optimizing the processes and exploring new designs. However, seeking advantage of this approach is faced with three major challenges: tracking the movement of the interface, accurately reproducing the surface tension forces and, eventually, correctly describing the heat and mass transfer between the phases. Several numerical methods have been described in literature, broadly categorized as interface tracking and interface capturing methods. The former approach explicitly tracks the interface, for example, in boundary integral methods (Hou *et al.*, 2001) or front tracking methods (Tryggvason *et al.*, 2001). Alternatively, the dynamics of the interface can be implicitly captured using a scalar function such as in volume of fluid, level set or phase field method. These can be further classified as sharp and diffuse interface methods based on the representation of the interface. In sharp interface methods, like Volume of Fluid (VoF) or Moment of Fluid (MOF) (Asuri Mukundan *et al.*, 2020; Milcent and Lemoine, 2020), the interface is defined as a geometrical surface that separates the immiscible phases. However, these methods are known to break down when the interface thickness becomes of the order of the local radius of curvature (Hou *et al.*, 1997; Lowengrub and Truskinovsky, 1998). This can be addressed by smoothing the interface over a few grid cells for computational ease as in Level Set Method (LSM) (Osher and Sethian, 1988). One of the drawbacks of LSM is that it hardly conserves mass though several advancements have been proposed like coupling with VOF (Sussman, 2003; Sussman and Puckett, 2000) or the use of regularized characteristic function instead of reinitialization (Hong *et al.*, 2007; Olsson *et al.*, 2007). A comprehensive review of LSM can be found in the recent review article by Gibou *et al.* (Gibou *et al.*, 2018). Another method with a similar approach to spread the interface is the Phase-Field Method (PFM) or the Diffuse Interface Method (DIM) (Anderson *et al.*, 1998; Jacqmin, 1999; Kim, 2015; Lowengrub and Truskinovsky, 1998). However, contrary to LSM, the smoothing is inherently based on the interface thickness which is more of a physical parameter than merely a computational adjustment.

In the PFM, the interface is defined as a region of smooth transition of properties from one fluid (or phase) to another. This was first proposed by van der Waals (Rowlinson, 1979) and was later extended by Cahn and Hilliard (Cahn and Hilliard, 1958, 1959) where the authors derived an expression for the total free

energy of the inhomogeneous system taking into account the effects of local energy at the interface arising due to the gradient of mole fraction. The starting point of the PFM thus lies in identifying the system to be inhomogeneous *w.r.t* a certain variable, usually an intensive property (Cahn and Hilliard, 1958) such as density, termed as the phase-field variable,  $\phi$ . It is followed by describing the total free energy including the gradient terms as a functional of  $\phi$ . The physical constraints or conditions of the system change the total energy of the system which in turn will move towards the state of minimum energy (or maximum entropy) thereby altering the  $\phi$  field. As the variation of  $\phi$  represents the interface region, the movement of interface is therefore implicitly captured by the evolution of  $\phi$  using phase-field equations, such as the advected form of Cahn-Hilliard equation (Cahn and Hilliard, 1958, 1959) or Allen-Cahn equation (Allen and Cahn, 1972; Allen and Cahn, 1973), the former being primarily considered in literature owing to its conservative nature. The phase-field equation is coupled to the momentum conservation in Navier-Stokes equations via the Korteweg stress by expressing the surface tension force as the interface energy per unit area. This calls for two additional physical parameters, namely interface thickness ( $\xi$ ) and surface tension ( $\sigma$ ) to define the model. The coupled analysis of phase-field equation with hydrodynamics, *i.e.* Navier-Stokes/Cahn-Hilliard (NS-CH) was initially undertaken by Gurtin *et al.* (Gurtin *et al.*, 1996) following which several pioneering works, as eloquently described in the review works (Anderson *et al.*, 1998; Emmerich, 2008; Helmut Abels *et al.*, 2017; Kim, 2015), have led to noteworthy advancement of the subject (Guo and Lin, 2015; Magaletti *et al.*, 2013; Mirjalili *et al.*, 2020; Xu *et al.*, 2018). A wide range of problems in fluid mechanics have been analyzed using this method, such as coalescence of drops (Jacqmin, 1999), Faraday instabilities (Takagi and Matsumoto, 2011), contact angle and effect of variable wettability (Borcia *et al.*, 2008, 2014) and thermo-capillary phenomena (Antanovskii, 1995; Guo and Lin, 2015). One of the primary assumptions of the classical phase-field model is the incompressibility and uniform density of both the phases/components (Hohenberg and Halperin, 1977). While the former holds true in many cases, the latter is far from real systems. With Boussinesq approximation based approach being limited to small density ratios (Hua *et al.*, 2011), several modified models have illustrated systems with density ratio as high as 1000 (Boyer, 2002; Ding *et al.*, 2007; Lowengrub and Truskinovsky, 1998; Shen and Yang, 2010). This is a challenging numerical problem despite being frequently encountered in two-phase applications. A comparative study of these different models has been undertaken by (Aland and Voigt, 2012)).

Despite a rich literature on the subject supporting the aforesaid advantages, PFM has not been used extensively for physical problems as compared to its other counterparts such as VOF or LSM (A Mirjalili *et al.*). One of the most often cited drawbacks is the higher computational cost owing to the need of having

a minimum of 4-6 grid points in the interface region so as to accurately capture the evolution of  $\phi$  on a uniform computational grid, thus necessitating a finer mesh. This can however be addressed using adaptive mesh as discussed in the recent work of (Wang *et al.*, 2018)). Another challenge is the appropriate choice of the mobility parameter ( $M$ ) which appears in the Cahn-Hilliard equation, referred to as phase-field equation henceforth. As described in (Magaletti *et al.*, 2013), the mobility defines the mass diffusivity between the two phases occurring locally at the interface at a molecular scale and characterizes the timescale for attaining the equilibrium. The description in terms of time scales is of prime relevance to the current work and will be discussed in §6. In an abstract sense, it can also be understood as a diffusion coefficient of the potential (variation of the free energy functional with the phase-field variable). Several relations have been proposed for it in the literature (Jacqmin, 1999; Lowengrub and Truskinovsky, 1998; Magaletti *et al.*, 2013; Sibley *et al.*, 2013; Xu *et al.*, 2018; Yue *et al.*, 2010) in terms of dimensionless quantities, namely Peclet number ( $Pe \propto \xi/M\sigma$ ) and Cahn number  $Cn = \frac{\xi}{L}$ , where  $\xi$  is the interface thickness,  $\sigma$  is the surface tension coefficient and  $L$  is the characteristic length, primarily using matched asymptotic analysis. This ensures the PFM approaching the sharp interface limit when the interface thickness tends to zero. The problem has been investigated more intensively in the recent works of (Magaletti *et al.*, 2013), (Xu *et al.*, 2018), and (Mirjalili *et al.*, 2020). (Magaletti *et al.*, 2013) presented a summary of existing relations whilst highlighting that a general method to appropriately choose the mobility parameter is lacking in literature. One of the striking features of their work has been to consider a multi-scale time analysis accounting for different dynamic scales involved in PFM. **Based on their analytical analysis, they scaled the mobility parameter and defined it in the form of a dimensionless number,  $M^*$ . This was termed as the mobility number and was expressed in terms of the Cahn-number as  $M^* = \alpha Cn^2$ , where  $\alpha$  is an appropriate constant. A better understanding of this number can be sought in terms of  $Pe$  which can be expressed as  $Cn/M^*$ .** Based on their elementary test cases,  $\alpha = 3$  was found as the optimum value. However, using this relation for real physical systems is not so straightforward primarily due to different possibilities of characteristic velocity scales to choose from. This has been aptly highlighted in the recent work of (Kajzer and Pozorski, 2020). Opting for maximum velocity in the domain as the velocity scale, they introduced another numerical factor termed as safety factor to ensure that mobility is not over estimated. In our perspective, this still makes the model dependent on an unknown numerical parameter and brings an element of uncertainty about the accuracy of the results obtained with PFM, especially when no a priori estimates are available for validation with experimental or analytical data. Even after validating with a certain value of mobility, it is likely that changing a set of physical parameters of a system may cause the solution to become erroneous for the same value.

In the current work, we address this issue by developing a method wherein we follow an innovative approach to evaluate the local interface thickness (in space and time) in terms of the gradient of the phase-field variable assuming the interface is in local equilibrium. In doing so, we implicitly consider each computational volume as an isolated entity *w.r.t* phase-field equation which permits to choose local velocity as the velocity scale in the mobility relation proposed in (Magaletti *et al.*, 2013). We call this method as adaptive interface thickness based mobility approach for the phase-field method (AITM-PFM) which makes the PFM less dependent on the choice of mobility or any other numerical parameter rendering it more robust. The article is organized as follows. We first describe the usual phase-field model followed by presenting the AITM-PFM. The mathematical and numerical method used in the current work are then described. Subsequently, the validation of the current numerical model is presented for canonical cases followed by the case of the rise of a lighter bubble in a heavier medium (density ratio 10 and 1000) highlighting the dependence of outcome on mobility in the usual PFM. We then demonstrate the robustness of the developed methodology for different other test cases, Rayleigh-Taylor instability, axisymmetric bubble rise and bubble coalescence.

## 2. Phase field method

Consider a two-phase system which is inhomogeneous *w.r.t* the phase-field variable,  $\phi$ . The free energy of the system per unit volume ( $F_V$ ), as discussed in (Cahn and Hilliard, 1958, 1959), can be described as,

$$F_V = \beta f(\phi) + \frac{\alpha}{2} |\nabla \phi|^2 \quad (1)$$

where, the first term represents the bulk free energy *i.e.* due to pure phases while the second denotes the gradient of energy arising from the interface region. The parameters  $\alpha$  and  $\beta$  are related to the physical variables, surface tension ( $\sigma$ ) and interface thickness ( $\xi$ ). Further,  $f$  is represented by a double well function where the minima of the function (0 and 1 in the present case) represent the pure two phases as shown in **Error! Reference source not found.**. The system will rest in a state to minimize its free energy (Cahn and Hilliard, 1958, 1959), which can be mathematically described by the variation of energy functional,  $F_V$  *w.r.t*  $\phi$  as,

$$\eta = \frac{\delta F_V}{\delta \phi} = \beta \frac{\partial f}{\partial \phi} - \nabla \cdot (\alpha \nabla \phi) \quad (2)$$

where,  $\eta$  denotes the chemical potential.

The minimization condition yields a vanishing chemical potential, *i. e.*,  $\eta = 0$ , which can be further reduced to equal contribution of bulk and gradient of energy,  $\beta \frac{\partial f}{\partial \phi} = \nabla \cdot (\alpha \nabla \phi)$  at the equilibrium state. This can be elucidated in physical sense as follows. Any departure from the initial equilibrium state will increase the energy of the system. For instance, the spread (diffusion) of the interface will lead to a higher contribution of the bulk free energy. This will be counteracted upon by the gradient term driving the interface to become sharper, thus increasing its contribution to restore the equilibrium. The condition of vanishing chemical potential can be further modified to derive the expression for surface tension which in a 1D case is given by  $\sigma = \int_{-\infty}^{\infty} (\beta f) dx$ . This can be further simplified to yield a relation for  $\alpha$  and  $\beta$  in terms of surface tension  $\sigma$  and interface thickness  $\xi$  as,

$$\alpha = 3\sqrt{2}\sigma\xi, \quad \beta = 3\sqrt{2}\frac{\sigma}{\xi} \quad (3)$$

In addition, we can also define  $\phi$  at equilibrium in a 1D profile as,

$$\phi = \frac{1}{2} + \frac{1}{2} \tanh \sqrt{\frac{\beta}{\alpha}} \frac{X}{\sqrt{2}} \quad (4)$$

where  $X = x - 0.5$  in order to be coherent with the choice of  $\phi = 0$  and 1 representing the bulk phases. It can be extended to higher dimensions in a direction normal to the interface. This is a major advantage of PFM where an infinitely derivable smooth function is used. The departure from an equilibrium state of a physical system occurs primarily due to the movement of the underlying phase and thus the interface. To capture this motion, the phase-field variable is subjected to an advection equation, as encountered in usual flow equations. Owing to its property to conserve the phase-field parameter, we consider the advected form of Cahn Hilliard (CH) equation in the present work as defined below, whose right-hand side plays the role of maintaining equilibrium at the interface,

$$\frac{\partial \phi}{\partial t} + \mathbf{V} \cdot \nabla \phi = \nabla \cdot (M \nabla \eta) \quad (5)$$

Here,  $M$  represents the mobility parameter. **In the non-dimensional form (Ding *et al.*, 2007), it appears in the  $Pe$  which for the current form of equations can be written as  $Pe = UL/M\beta$ .** This also helps to define the characteristic time scale of CH equation which is analogous to the fast time scale in inner layer

(interface region) considered in (Magaletti *et al.*, 2013). It can be interpreted as the time scale at which the equilibrium of the interface is attained or restored when it deviates from its equilibrium state. The similarity of CH equation to the diffusion equation, the diffusion variable being the chemical potential rather than  $\phi$  itself, makes it possible to define CH time scale as  $t_\phi \propto \frac{1}{M}$ . In the present work, we consider mobility of the form  $M = M_0\phi(1 - \phi)$ ,  $M_0$  being a constant factor. This particular choice ensures that the phase-field equation acts only in the interface region and circumvents the possibility of any artificial diffusion arising in the bulk. This is further motivated from the work of (Sibley *et al.*, 2013) in which, using matched asymptotic analysis, the authors have shown that a variable mobility helps to recover the classical pressure jump condition at the interface even when the bulk may not be in equilibrium. This helps to impede any numerical artifact as numerical limitations may not lead to exactly vanishing chemical potential in the bulk, especially near the interface region causing an erroneous pressure field.

The phase-field equation is coupled to the Navier-Stokes by adding a surface tension force defined in terms of phase-field variable. This has been presented in literature in stress as well as in potential form. Herein, we chose the potential form (Badalassi *et al.*, 2003; Ding *et al.*, 2007; Sibley *et al.*, 2013), owing to its ease in numerical implementation, which in case of incompressible flow systems can be written as,

$$F_\sigma = \eta \nabla \phi \quad (6)$$

The form of expression given in Eq. (6) can be further written as  $\nabla F_V - \alpha(\nabla \phi \otimes \nabla \phi)$ , where the latter term is known as Korteweg stress. It is worth mentioning that several variations of this force have been presented in literature as summarized by (Sibley *et al.*, 2013) owing to different methodologies followed to derive the expression. The general expression for these terms which appear along with expression in Eq. (6) in the framework of current study can be written as,  $-\mathcal{B}\nabla(\beta f(\phi)) + \mathcal{G}\frac{\alpha}{4}|\nabla \phi|^2$  where different values of  $\mathcal{B}$  and  $\mathcal{G}$  represent different models considered in literature as summarized in (Sibley *et al.*, 2013) (for example,  $\mathcal{B} = 1$  and  $\mathcal{G} = -2$  yield the model by (Jacqmin, 1999)). In several works, these additional terms are sometimes included in the pressure term and the pressure term appearing in the momentum equation is thus termed as modified pressure. However, it is not clear whether the pressure used for post processing the numerical experiments is the modified pressure or the usual mechanical pressure. In order to avoid any ambiguities, we keep the pressure in the momentum equation as the mechanical pressure and let these additional terms go explicitly into the momentum equation as considered by (Jacqmin, 1999) and described in (Sibley *et al.*, 2013),

$$F_{\sigma,A} = \nabla(\beta f(\phi) - \frac{\alpha}{2} |\nabla\phi|^2) \quad (7)$$

where subscript  $A$  refers to additional terms. Thus, the total force due to phase-field, termed as surface tension force ( $F_{ST}$ ) henceforth is,

$$F_{ST} = F_{\sigma} + F_{\sigma,A} = \eta \nabla\phi + \nabla(\beta f(\phi) - \frac{\alpha}{2} |\nabla\phi|^2) \quad (8)$$

### 3. Adaptive interface thickness based mobility (AITM-PFM)

The previous section described the phase-field model as has been discussed in the literature. We now present our approach to obtain appropriate mobility using the relation described in (Magaletti *et al.*, 2013). Herein, we develop the theoretical background while test cases will be demonstrated in §7. Several authors have presented relationships using matched asymptotic analysis when the Cahn number ( $Cn$ ) tends to zero (Jacqmin, 1999; Lowengrub and Truskinovsky, 1998; Magaletti *et al.*, 2013; Sibley *et al.*, 2013; Xu *et al.*, 2018; Yue *et al.*, 2010). These are obtained at a fixed  $Cn$  (both in space and time) and thus it can be inferred that the derived appropriate value of mobility, at least in principle, will ensure that the initial  $Cn$  is maintained throughout the simulation along the perimeter of the interface thereby sustaining the equilibrium state. However, this is faced with two major challenges. Firstly, in an event of large topological changes, such as in Faraday or Rayleigh-Taylor instabilities or breakup/coalescence of drops, despite making the closest appropriate choice of mobility, the interface thickness across the entire perimeter may not be exactly preserved and may vary locally in space (and/or time). This may lead to over or under estimation of the value of mobility for that given local interface thickness and may gradually increase the error over a period of time especially when studying a long-term behavior. Among different possible solutions, one could develop a similar relation whilst considering  $Cn$  as a field. Not ruling out the possibility to attain better results with this methodology, the analysis will however be highly complicated and exhaustive. Secondly, as was described in §1, the proposed relations in the literature involve a velocity scale (or  $Pe$ ), which in a dimensional system will always lead to an ambiguity to choose the appropriate velocity scale. Nevertheless, not repudiating the possibility to have such a suitable scale for a given problem, this will still call for some trial and error to rely upon the solution. For instance, the authors in (Kajzer and Pozorski, 2020) used the relation proposed by (Magaletti *et al.*, 2013) in the dimensional form as,

$$M_o \cong \frac{\xi^2 U}{\sigma} \quad (9)$$

Here,  $U$  is characteristic velocity or velocity scale for a given physical system. The authors used maximum velocity in the domain for  $U$  but ended up by introducing another numerical factor, termed as safety factor in order to prevent the over-estimation of the mobility. Though it opens up the possibility to use the analytical relation in a more practical sense, we believe it still relies on a numerical (safety) parameter to have the correct results thereby raising concerns over the fidelity of the solution in the absence of any benchmark cases, especially when using the method for industrial problems such as exploring new designs or optimization studies.

In order to derive an alternate approach, we begin by assuming that the interface is in “local” equilibrium. The emphasis on the word “local” denotes the condition that each point in the interface region is in equilibrium. The significance of assuming the local equilibrium is two folds. Firstly, as we only know  $\phi$  profile under equilibrium conditions (as given in Eq. (4)), the corresponding interface thickness can thus be reverse calculated only under the aforementioned assumption. Secondly, by assuming the local equilibrium, each computational grid point/sub-volume can be considered as an isolated or a separate entity and the problem thus boils down to find the appropriate local mobility. In such a scenario, knowing the local “equilibrium” interface thickness (as described below), the local velocity becomes an obvious choice to be considered in the mobility relation (Eq. (9)) removing any ambiguity in defining the velocity scale. Thus, we have narrowed down the overall problem to evaluate this local interface thickness which is the highlight of the current work and is described below.

Consider a 1D case for the sake of simplicity and a straightforward extension follows in higher dimensions. The initial interface profile at  $t = 0$ , with interface thickness  $\xi_0$  at equilibrium can be written as described by Eq. (4),

$$\phi_0 = \frac{1}{2} + \frac{1}{2} \tanh\left(\frac{x-0.5}{\xi_0 \sqrt{2}}\right) \quad (10)$$

where  $\xi_0 = \sqrt{\frac{\alpha_0}{\beta_0}}$ . The equilibrium slope at any point  $x$  can be written as,

$$m_{x,0} = \frac{d\phi_0}{dx} = \frac{1}{2\sqrt{2}\xi_0} \operatorname{sech}^2\left(\frac{x-0.5}{\xi_0 \sqrt{2}}\right) \quad (11)$$

As the system evolves, the interface topology/thickness will tend to change locally (contract or diffuse) thereby deviating from the equilibrium state and our objective is to restore it back via an appropriate value of the mobility. For the sake of illustration, let us consider that the interface contracts and the interface thickness tend to become  $\xi_t$  such that  $\xi_0 > \xi_t$  with  $\phi$  profile as shown in **Error! Reference source not found.** Herein the slope at same point  $x$  can be evaluated from Eq. (11) with  $\xi_0$  replaced by  $\xi_t$  (or  $\xi^{(n)}(x)$  to be coherent with numerical terminology and representing the interface thickness at the end of iteration). Further, let  $\phi^{(n)}(x)$  denote the  $\phi$  field at the end of  $n^{th}$  iteration. The assumption of local equilibrium as mentioned before further implies that the relation for the interface thickness and the slope as given by Eq. (10) and Eq. (11) will be valid throughout, both in space and time, which may not be true otherwise. A simple algebraic manipulation to eliminate  $(x - 0.5)$  from Eq. (10) and Eq. (11) yields,

$$\xi^{(n)}(x) = \frac{1}{2\sqrt{2} \left( \frac{d(\phi^{(n)}(x))}{dx} \right)} \operatorname{sech}^2 \left( \tanh^{-1} (2\phi^{(n)}(x) - 1) \right) \quad (12)$$

The above Eq. (12) thus describes the local equilibrium thickness at any  $x$  in terms of local slope,  $\frac{d(\phi^{(n)}(x))}{dx}$ , which can be evaluated numerically from the  $\phi^{(n)}(x)$  field. In physical terms, it can be interpreted as the interface thickness which would persist if we had the given  $\phi$  –field. Using this in Eq. (9), we can thus write the mobility as,

$$M_o^{(n+1)} = \frac{\xi^{(n)2} U^{(n)}}{\sigma} \quad (13)$$

Here,  $U$  represents the local velocity magnitude. It is to be mentioned here that the proportionality constant proposed in (Magaletti *et al.*, 2013) was based on certain test cases only. Further, as themselves quoted by the authors that the proposed relation will ensure that dynamics of sharp interface are retained in the limit of vanishing Cahn number and the proportionality constant could play a role in numerical stability, we stick to the relation as in Eq. (13) to circumvent any ambiguities creeping into the model. **This ensures that the proposed model does not depend on any numerical parameter controlling the outcome of the simulation.** The initial value of mobility, *i.e.* at  $t = 0$ , is taken to be very small referring to the value which ensures negligible parasitic currents. This can be estimated using the initial interface thickness in Eq. (13) following which the appropriate value is obtained locally based on how the system evolves. Since we adapt the local interface thickness to have the appropriate value of mobility, we have defined this methodology as adaptive interface thickness based mobility – phase field method (AITM-PFM). It is to be noted here that the calculated interface thickness is only used to evaluate the appropriate value of

mobility and does not imply that the actual interface thickness has changed and thus the parameters  $\alpha$  and  $\beta$  remain constant. In fact, the idea of adaptive interface thickness to calculate the mobility is to ensure that initial interface thickness is retained by adapting mobility locally based on changes in the local interface profile.

#### 4. Mathematical model for two-phase system

We consider classical Navier-Stokes equation for incompressible fluids comprising of conservation of mass and momentum in addition to CH equation (Eq.(5)) as described above. Thus, the complete set of governing equations can be written as,

$$\nabla \cdot \mathbf{V} = 0 \quad (14)$$

$$\rho \left( \frac{\partial \mathbf{V}}{\partial t} + (\mathbf{V} \cdot \nabla) \mathbf{V} \right) = -\nabla P + \mu \nabla^2 \mathbf{V} + \mathbf{F}_{ST} + \mathbf{f}_{ext} \quad (15)$$

In Eq. (15),  $\mathbf{f}_{ext}$  stands for external volumetric forces such as gravity while  $\mathbf{F}_{ST}$  denotes surface tension force given by Eq. (8). It is to be mentioned that owing to the choice of volume fraction as the phase-field parameter, the solenoidal velocity condition is attained as described in (Abels *et al.*, 2012; Ding *et al.*, 2007). The physical properties are calculated as a linear combination of volume fraction (phase-field parameter) as,

$$Y = Y_1 \phi + (1 - \phi) Y_2 \quad (16)$$

where,  $Y$  denotes density and viscosity.

#### 5. Numerical discretization

The governing equations described above representing a two-phase system are discretized using the finite volume method which is briefly presented in this section. These are solved using our open-source code Notus CFD (Coquerelle and Glockner, 2016; Desmons and Coquerelle, 2020; Jost *et al.*, 2020) which is based on structured staggered cartesian meshes. The code permits to use several discretization methods; we have chosen the ones that are most widely used for two-phase flow simulations in order to focus on

the PFM itself. One of the key features of the code is that it furnishes validated numerical models such as Level Set method (Coquerelle and Glockner, 2016) that has been used in this article for comparison. The code uses the well-known projection method introduced by (Chorin, 1967) where a prediction velocity is first computed from the momentum equation and then corrected to ensure incompressibility while the pressure is updated from the pressure increment obtained from the Poisson equation. As the momentum equation is solved prior to CH equation, the surface tension term in the momentum equation is evaluated based on  $\phi$  field at discrete time  $t^{(n)}$ .

The phase-field equation involves a fourth order derivative of the phase-field variable which makes it challenging for numerical discretization. Herein, we resort to implicit discretization using a second order central difference scheme for  $\nabla \cdot (M\nabla\eta)$  term which can be expanded to  $\nabla \cdot (M\nabla(4\beta\phi^3 - 6\beta\phi^2 + 2\beta\phi - \nabla \cdot (\alpha\nabla\phi)))$  for the form of free energy considered in the present work. Thus, we have chosen to numerically approximate this nonlinear term through the following linearization,

$$\nabla \cdot (M\nabla\eta) \simeq \nabla \cdot \left( M^{(n+1)} \nabla \left( 4\beta\phi^{2(n)}\phi^{(n+1)} - 6\beta\phi^{(n)}\phi^{(n+1)} + 2\beta\phi^{(n+1)} - \nabla \cdot (\alpha\nabla\phi^{(n+1)}) \right) \right) \quad (17)$$

As mentioned earlier,  $M$  is taken to be dependent on  $\phi$  which in Eq. (17) is evaluated explicitly as  $M^{(n+1)} \equiv M_0^{n+1}\phi^{(n)}(1 - \phi^{(n)})$  with  $M_0^{n+1}$  evaluated using the relation given by Eq.(13).

For temporal discretization, we resort to first order forward in time as,

$$\frac{\partial\phi}{\partial t} \simeq \frac{\phi^{(n+1)} - \phi^{(n)}}{\Delta t} \quad (18)$$

The advection term is integrated in time thanks to a second order Runge-Kutta Non-Strong Stability Preserving (RKNSSP32) explicit scheme, as suggested by (Wang and Spiteri, 2007) coupled with a fifth order Weighted Essentially Non-Oscillatory (WENO53) spatial scheme. This numerical method ensures high spatial as well as temporal precision for the transport of the interface. This is similar to the one considered in the work of (Ding *et al.*, 2007).

## 6. Results with constant Mobility and interface thickness

The presence of surface tension in a two-phase problem induces an additional force in the system whose effect has to be weighed against other prevalent forces (viscous, inertia, gravity etc.). The model should therefore be able to address a wide range of physical problems. Different canonical test cases, as considered in the literature, are presented in the current work to account for different effects. We divide these test cases into two categories, validation studies wherein we describe elementary cases whilst considering constant mobility  $M_o$  in order to validate the current model and numerical scheme (§6.1 and §6.2). Subsequently, we consider more stringent studies involving topological changes of the interface and highlighting the limitations with constant  $M_o$  (§6.3) followed by demonstrating AITM-PFM (§7).

In all these studies, the time step for simulation is taken to be  $10^{-3}s$  **unless mentioned otherwise**. A uniform grid is used in the entire 2D domain, both in  $x$  and  $y$  directions, which is defined based on the number of grid points in the initial interface thickness,  $N_g$ , as  $\Delta x = \Delta y = \xi/N_g$ . It is worth mentioning that the interface thickness has been interpreted in different ways in the literature. For instance, (Jacqmin, 1999) defined it as a region of 90% variation of  $\phi$ . In the context of current work, it refers to the region where  $\phi$  varies from 0.05 to 0.95. For the sake of clarity, we prefer to term it as computational interface thickness. However, to the best of our understanding, this definition holds relevance to define the number of grid points in the interface as also pointed out by (Magaletti *et al.*, 2013). For instance, defining  $N_g$  grid points in computational interface thickness (defined by 90% cut off) will actually lead to  $4N_g$  grid points in the region of complete variation of  $\phi$  from 0 to 1 within the presented framework. In order to avoid any confusion, we refer to interface thickness and not computational interface thickness when defining the grid size as per the aforementioned relation. Nevertheless, it can be safely ascertained that if the latter is considered, a higher spatial resolution and thus, more accurate results than presented herein can be attained. It is to be mentioned here that in order to prevent over and under shoot of the phase-field variable from its bounds 0 and 1, we ensure that the phase-field function remains bounded by setting  $\phi = 0$  and  $\phi = 1$  if  $\phi < \varepsilon$  and  $\phi > 1 - \varepsilon$  where  $\varepsilon = 10^{-9}$ . Though it may be argued that the underlying numerical schemes should be able to ensure the boundedness, our numerical tests show satisfactory agreement with results from literature rendering our approach simpler.

## 6.1 Bubble/droplet in equilibrium

Consider a drop of one fluid phase which is suspended in another phase as shown in **Error! Reference source not found**. and is at rest in equilibrium (*i. e.*  $U_0 = 0$ ). In the absence of any external force, the

pressure difference between the two phases is balanced by the surface tension and is given by the Young-Laplace pressure jump in 2D:  $\Delta P = \sigma/R$ , where  $R=D/2$  is the radius of the drop. The implementation of surface tension force is known to yield non-physical velocity fields, termed as spurious or parasitic currents, in the system, originating in the interfacial region. These arise due to discretization errors in the numerical schemes or numerical parameters used in the model, such as mobility in the PFM. These are further enhanced with the increase in density difference of the two phases and surface tension coefficient. In convection dominated problems their interference with physical velocities may lead to erroneous results depending on their relative magnitude. Nevertheless, an ideal case would be to have vanishing parasitic currents.

In the current work, we evaluate the spurious currents generated as a function of  $Cn$  and number of grid points in the interface ( $N_g$ ). This implicitly represents the interface thickness and the grid size, respectively along with the mobility. We consider two different cases, first with both phases having the same density as considered in (Mirjalili *et al.*, 2019) and second, with density ratio 1000. This particular choice of high-density ratio is motivated to account for various problems resembling to air-water physical system. Viscosity is the same for both the phases and is taken to be  $0.1 Pa.s$ . As in (Coquerelle and Glockner, 2016; Mirjalili *et al.*, 2019), Laplace number (ratio between surface tension and momentum transport, represented by  $La = (\sigma\rho D)/\mu^2$ ) is used to characterize the current problem. For the case of different densities of the two phases,  $\rho$  in  $La$  refers to the mean density. The highest  $La$  considered are  $1.2 \times 10^4$  and  $7.84 \times 10^4$  for the cases of same and different densities, respectively. Further, the simulations are run for dimensionless time  $t^* = \frac{\sigma t}{\mu D} = 250$  as also considered in (Mirjalili *et al.*, 2019) as it gives ample time for any spurious currents to dampen out due to viscous effects. As viscous and surface tension are the primary forces in this case, the outputs are compared in terms of Capillary number ( $Ca = \frac{U_{max}\mu}{\sigma}$ ). **Error! Reference source not found.** shows the evolution of  $Ca$  for  $Cn = 0.1$  and grid sizes  $100 \times 100$ ,  $200 \times 200$  and  $400 \times 400$  which correspond to  $N_g = 4, 8$  and  $16$ , respectively for  $M_0 = 10^{-5}$  and  $10^{-10}$ . While in both cases of mobility, the spurious currents seem to converge, a higher value leads to greater spurious currents which can be explained as follows. Despite initializing with an equilibrium profile at  $t = 0$ , the numerical inaccuracies and precision cause imbalance in the equilibrium state. A higher value of mobility implies more diffusion to counter this imbalance causing higher spurious currents. A similar reasoning can be cited for its lower value and is evident from the trend for  $M_0 = 10^{-10}$ .

We further compare  $Ca$  at  $t^* = 250$  for different  $Cn = \frac{\xi}{D}$  and  $N_g$  as shown in **Error! Reference source not found.** Herein, we have shown results for uniform density and density ratio of 1000. The observed trend is on expected lines wherein reducing the interface thickness and adding more grid points in the interface result in minimizing the spurious effects reflected from lower values of  $Ca$ . We further verify the Young Laplace relation and evaluate the error in surface tension obtained from numerical computations as,

$$\epsilon_{error} = \frac{|\sigma_{actual} - \sigma_{numerical}|}{\sigma_{actual}} \times 100 \quad (19)$$

Here,  $\sigma_{numerical}$  is evaluated using the Young Laplace relation with  $\Delta P$  representing the difference in average pressure inside and outside the bubble and  $\sigma_{actual} = 1 \text{ N/m}$  is the imposed value in the simulation. An important point to be highlighted here is how to define the inside and outside of the bubble. Considering the definition based on 90% cut off as in (Jacqmin, 1999) thereby implying  $\phi > 0.95$  as interior region of the bubble and  $\phi < 0.05$  as exterior, we obtain  $\epsilon_{error} \approx 1.87 \%$  for  $Cn = 0.1$  with  $N_g = 4$ . However, the same gives  $\epsilon_{error} \approx 13 \%$  when  $\phi = 0.5$  was considered to define interior and exterior of the bubble. Thus, while it may be intuitive to consider  $\phi = 0.5$  as the position of the interface, it will be more judicious to define average properties based on the definition of bulk as proposed in (Jacqmin, 1999). The assertion can be further reasoned to the fact that the interface region merely represents a transition zone from one bulk phase to another one and thus can be excluded to be a part of bulk fluid region.

## 6.2 Advection of bubble/droplet

Extending the validation studies, we consider another canonical test case in which the whole domain is advected with a certain velocity, the schematic being the same as shown in **Error! Reference source not found.** except that  $U_o$  has now some finite value. Though being far from a realistic system, it provides a means to demonstrate the coupling between NVS and CH equations in a more rigorous manner as the finite velocity field will have more stringent impact on the evolution of the pressure field, especially near the interface region. Nevertheless, the problem in a physical sense can be sought as an equivalent to a droplet (or a bubble) in equilibrium when seen from the reference frame of the fluid and thus it is expected that the initial profiles of the flow variables will be unaffected. However, advecting the interface may lead to numerical errors owing to the discretization method, grid size, etc. whose accrual over time may cause

erroneous outputs. We analyze the impact of advection velocity on the interface profile after one advection period as considered in (Mirjalili *et al.*, 2020). In addition, the analysis is also extended to a wider range of velocities.

They characterized the problem by splitting the contribution of error in two categories, namely, the deviation from an ideal sharp interface profile ( $E_\xi$ ) and secondly, as  $E_\Delta = \phi(t = T, x, y) - \phi(t = 0, x, y)$ , where  $T$  is time period of advection and is related to advection velocity as  $T = L/U_0$  with  $L = 1 \text{ m}$  in the present case. Herein, we focus on  $E_\Delta$  which implicitly represents the impact of grid size or  $N_g$  and is evaluated using the following expression,

$$\|E_\Delta\|_2 = \|\phi(T, x, y) - \phi(0, x, y)\|_2 \quad (20)$$

where  $\|\cdot\|_2$  denotes the  $L_2$  norm. The time simulation is performed with time step of  $10^{-4} \text{ s}$  and mobility  $M_0 = 10^{-10}$ . The choice of mobility is driven from the fact that the current case refers to a state of equilibrium and thus a lower value aids to maintain it as was shown in §6.1.

**Error! Reference source not found.** shows  $\|E_\Delta\|_2$  for  $U_0 = 1 \text{ ms}^{-1}$ ,  $25 \text{ ms}^{-1}$  and  $50 \text{ ms}^{-1}$  as a function of  $N_g = 4, 8, 16$  and  $32$  for  $Cn = 0.1$  and  $0.05$ . An increase in advection velocity causes the interface profile to deteriorate which can however be circumvented upon grid refinement (increasing  $N_g$ ) and is supported from observations in **Error! Reference source not found.** It also illustrates the effect of decreasing  $Cn$  at a constant  $N_g$  and it can be inferred that a sharper interface profile requires a higher number of grid points to have a better or a same order of accuracy. This arises by virtue of sharper gradients which are more prone to inaccuracies in numerical precision and thus needs a smoother transition which is attained by a finer mesh. This also highlights one the challenging aspect of PFM approach, *i. e.* a smaller  $Cn$  number is essential to approach the sharp interface limit which may however necessitate more grid points to reduce the influence of numerical errors.

We further extend the analysis over several periods of advection in order to study the impact of numerical errors over a long duration, a feature relevant to real systems. We restrict this investigation to the case with uniform density in order to demonstrate the impact of errors even on such a simple system. Herein, the computation is performed until the time  $t = 4 \text{ s}$  with an advection velocity of  $U_0 = 1 \text{ m} \cdot \text{s}^{-1}$  whilst the other parameters are same as mentioned above. We first compare the phase field and pressure profiles at  $t = 4 \text{ s}$  for  $N_g = 4$  and  $8$  and at  $y = 0.5 \text{ m}$  plane (see **Error! Reference source not found.**).

We observe a smooth transition in both the profiles for both the cases. Upon increasing the advection velocity  $U_0$  to  $25 \text{ m.s}^{-1}$ , an interesting behavior is observed wherein even though the interface profile nearly retains its smooth transition from one phase to another, the pressure profile near the onset and at the end of the interface region gets distorted for  $N_g = 4$  which vanishes upon increasing the number of grid points ( $N_g = 16$ ) as depicted in **Error! Reference source not found.** . A similar observation has been made in (Mirjalili *et al.*, 2020) in the  $\phi$  profile. The result presented here is therefore even more intriguing as it can be ascertained that despite the interface profile retaining its shape, an unrealistic pressure field can be developed near the interface due to numerical inaccuracies. In order to ascertain whether it is also a model limitation, we compare it with the pressure profile from the model of (Jacqmin, 1999) (see Eq. (7)) which is illustrated in **Error! Reference source not found.**. It is found that the unrealistic pressure profile (jump and fall near the interface region) nearly disappears except in the encircled region. We can thus deduce the following from these observations. Firstly, it is essential to account for the additional terms in the governing equations which help to ensure that any deviation from the equilibrium profile is restored thereby providing a sharp interface like pressure jump condition. This is coherent with the analytical demonstration in (Sibley *et al.*, 2013). We would like to mention here that due to the absence of any explicit quote in the literature to use the modified pressure or to consider additional terms in the model, it thus became inevitable to compare these models to bring out clarity on the subject.

The second observation pertains to a small kink as highlighted in **Error! Reference source not found.** which shows that even though the model has well accounted for additional terms to ensure equilibrium, the sharp interface pressure jump condition may be violated due to numerical inaccuracies which, nevertheless, can be improved upon by refining the mesh.

### 6.3 Rise of a lighter fluid bubble in a heavier fluid

Unlike the presented cases so far, most real systems involve change in the topology of the interface thereby disturbing the equipotential state. In such scenarios, mobility acts to restore the equilibrium state and in principle, it needs to be attained at the time scale of other physical mechanisms. In order to demonstrate this, we analyze a system comprising of a bubble of a lighter fluid rising in a heavier medium under the action of gravity.

**Error! Reference source not found.** shows the schematic of the problem while the fluid properties are as follows,  $\rho_1 = 100 \text{ kg.m}^{-3}$ ,  $\rho_2 = 1000 \text{ kg.m}^{-3}$ ,  $\mu_1 = 1 \text{ Pa.s}$ ,  $\mu_2 = 10 \text{ Pa.s}$  and  $\sigma = 24.5 \text{ N.m}^{-1}$ . The system configuration is similar to the one considered in (Coquerelle and Glockner, 2016; Hysing *et al.*,

2009). The Cahn number in the present case, defined as  $\xi/D$ , is taken to be 0.04. The model used in this test case (and for other cases henceforth) accounts for additional terms as described in Eq.(7) owing to their role as illustrated in the previous section. The results are compared in terms of the position of the bubble as well as the pressure field at various time instances which have been obtained from LSM as described in (Coquerelle and Glockner, 2016). One of the prime reasons for our interest in comparing the latter is to analyze how well the pressure jump condition evolves in the PFM when compared with sharp interface model and the effect of mobility on the same. Further, the absence of any such presentation in the literature, to the best of authors' knowledge, motivates such a comparison thereby imposing a more stringent analysis of the model.

**Error! Reference source not found.** shows the position of the bubble for different values of mobility at  $t = 3 s$  while the pressure profile is illustrated in **Error! Reference source not found.**. In order to understand this behavior, we plot the position of the bubble at various time instances as shown in **Error! Reference source not found.** for  $M_o = 10^{-10}$ .

As the bubble rises, the interface region on the leading side (facing the top surface) reduces in thickness whereas the trailing side becomes thicker as highlighted in **Error! Reference source not found.**. While the overall interface region is conserved, it is important to highlight that the thickness of the interface region along the perimeter is no longer uniform as was at  $t = 0$ . This is however obtained using a higher value of mobility,  $M_o = 10^{-5}$  as can be seen in **Error! Reference source not found.**. A higher value implies a smaller time scale of relaxation ( $t_\phi \propto 1/M$ ) and thus the interface dynamics is able to match the time scale of the bulk phenomenon, *i. e.* bubble rise due to density difference in this case. A close match of the PFM with LSM (**Error! Reference source not found.** and **Error! Reference source not found.** ) further validates our argument. It is noteworthy that there exists an upper limit to the value of mobility as a higher value can lead to more diffusion (numerical) and thereby distorting the interface. Thus, it can be inferred that accurate results with PFM are obtained only for a certain range of mobility illustrating its strong influence on the results. Even within that range of mobility, the results may slightly differ which in the absence of any benchmark case can cause ambiguity about the fidelity of the solutions.

The test case thus highlights the limitation of the PFM model in current form as the value of mobility has to be chosen by trial and error to match against certain benchmark cases. A similar argument will hold if we chose from different velocity scales in Eq. (13). It is important to mention here that various velocity scales may not even lead to stable numerical solution and one may have to introduce a scaling factor as

highlighted in (Kajzer and Pozorski, 2020). In order to overcome this, the AITM-PFM as described in §3 has been developed in the current work and test cases with this approach are presented in the next section.

## 7. Test cases with AITM-PFM

### 7.1 Bubble rise revisited

We begin demonstrating test cases with AITM-PFM approach initially for the same problem as described in §6.3 followed by a similar problem but with a higher density ratio to emphasize the robustness of the approach. **Error! Reference source not found.** shows the position of the interface (marked with  $\phi = 0.5$  contour) and pressure profile for  $Cn = 0.02$  and  $N_g = 5$  (test case as in §6.3) wherein the solution is found to match quite well with that obtained from LSM. The initial value of mobility is set to  $M_0 = 10^{-10}$  to ensure minimal spurious currents at the first iteration following which it changes as per the local adaptive interface thickness as described by Eq. (9). **Error! Reference source not found.** shows the position of the bubble at various time instances for the same case and it can be observed that the thickness of the interface region along the perimeter is preserved.

We further illustrate the evolution of  $M_0$  in **Error! Reference source not found.** in order to provide insights of the proposed method. For the sake of clarity, the contour plots have been shown only in the interface region defined by  $\phi \in [0.05, 0.95]$ . As governed by the dynamics of the bubble rise, the velocity of the leading edge is smaller as compared to the trailing edge (Chen *et al.*, 1999; Tripathi *et al.*, 2015) owing to a higher-pressure gradient at the latter. It can thereby be ascertained that the interface will advect at a faster speed at the trailing edge. Thus, in order to ensure that equilibrium in the interface is attained within the same time, a higher value of mobility at the trailing edge as compared to the leading edge is expected in order to balance the respective advection rate (higher mobility implying higher diffusion). The contour plots shown in **Error! Reference source not found.** are coherent with the proposed explanation. It is important to reiterate here that in the current method, each control volume is considered to be an independent entity, thanks to the local interface thickness as defined by Eq. (12). Thus, the mobility required to attain equilibrium in the interface is at local scale and therefore governed by local advection dynamics. This is different from the case of constant mobility wherein the entire interface region is considered to be a single entity and is driven towards equilibrium by a global value. Thus, a lower mobility at the leading edge which was decreasing in thickness is counter-intuitive but holds true as in the present

study, we are focused on considering the interface in the form of a locally independent entity to attain equilibrium.

We also compare the velocity of the bubble rise which is shown in **Error! Reference source not found.** with the average velocity of bubble rise defined by,

$$V_c = \left( \frac{\sum(\phi v)\Delta V}{\sum \phi \Delta V} \right)_{\phi > 0.95} \quad (21)$$

where,  $v$  is the y component of the velocity and  $\Delta V$  is the cell volume. Herein, we consider  $\phi > 0.95$  to be in coherence with the definition of interface region ( $0.05 < \phi < 0.95$ ) and thus the aforesaid expression representing the interior of the bubble. A close match between the profiles from the current method and LSM further validates the model.

We extend to test our approach for a similar system with the density ratio between the heavier and the lighter fluid being 1000. The physical properties of the fluids considered are as follows  $\rho_1 = 1 \text{ kg.m}^{-3}$ ,  $\rho_2 = 1000 \text{ kg.m}^{-3}$ ,  $\mu_1 = 0.1 \text{ Pa.s}$ ,  $\mu_2 = 10 \text{ Pa.s}$  and  $\sigma = 1.96 \text{ N.m}^{-1}$  (Coquerelle and Glockner, 2016; Hysing *et al.*, 2009). The significance of this test case lies to demonstrate the strength of the proposed methodology (AITM-PFM as well as numerical) for large density difference systems which are usually encountered in many real-world applications. We compare the position of the bubble at various time instances in **Error! Reference source not found.** A close coherence between the LSM and our approach validates our methodology. A further justification is illustrated by comparing the pressure profiles at  $x = 0.5 \text{ m}$  plane at various time intervals as depicted in **Error! Reference source not found.**

## 7.2 Rayleigh Taylor Instability

As a second test case, we analyze the system corresponding to Rayleigh-Taylor instability as schematically shown in **Error! Reference source not found.** at  $t = 0 \text{ s}$ . This case is a well-known problem comprising of a heavier fluid resting over a lighter fluid in the presence of gravity. When the interface is slightly perturbed, the configuration becomes unstable and the heavier fluid moves into the lighter fluid and vice-versa. Herein, for validating and comparing the results with the literature, we consider same parameters as in (Haghshenas *et al.*, 2017; Zuzio and Estivaleres, 2011). The initial interface profile at  $t = 0 \text{ s}$  is given

by  $y_0 = \frac{H}{2} - A \cos\left(k\left(x - \frac{L}{2}\right)\right)$ , where  $H = 4m$ ,  $L = 1m$ ,  $k$  is wavenumber defined as  $2\pi/L$  and  $A$  is amplitude of perturbation taken to be  $0.05m$ . The  $\phi$  field at  $t = 0s$  is defined by,

$$\phi(x, y, 0) = \frac{1}{2} + \frac{1}{2} \tanh\left(\frac{y-y_0}{\sqrt{2}\xi}\right) \quad (22)$$

The other fluid properties are as follows,  $\rho_1 = 0.1694 kg.m^{-3}$ ,  $\rho_2 = 1.225 kg.m^{-3}$ ,  $\mu_1 = \mu_2 = 0.00313 Pa.s$  and  $\sigma = 0.001337 N.m^{-1}$ . The fluid densities correspond to Atwood number ( $At = \frac{\rho_1 - \rho_2}{\rho_1 + \rho_2}$ ) of 0.757. The simulation is performed with  $Cn(x, y, t = 0s) = \frac{\xi}{L} = 0.005$  and  $N_g = 5$ .

A comparison between the interface profile at various time steps using LSM and AITM-PFM is illustrated in **Error! Reference source not found.** and a close match is observed. A particular attention needs to be focused at  $t = 0.9s$  where similar filament structures were obtained as in case of LSM. This was attained with a lower value of  $Cn$  in order to approach the sharp interface limit. It is to be further mentioned that with  $Cn = 0.02$  at the same time, the results were slightly different. Instead of curved filaments, a more diffused plume was formed which can be understood by the fact that in order to capture finer structures, the interface thickness needs to be less than the structures themselves. The results, however, have not been shown for the sake of brevity but an explicit mention is necessary to highlight that in an event of slight mismatch obtained whilst using our approach, it is not the limitation of AITM-PFM but an inherent characteristic of PFM.

### 7.3 Axisymmetric bubble rise

The problems considered so far can be described as relatively simple problems as the only topological change in the interface was the change in length (*i.e.* change in perimeter). However, in several real-world problems, one may encounter even more complex topological changes such as splitting or merging of the interface region for instance in detachment or coalescence of drops, respectively. These are more challenging as we have formation (vanishing) of the new (old) interface followed by capturing the dynamics of these new entities. In this section, we consider the problem of axisymmetric bubble rise as considered in (Ding *et al.*, 2007; Sussman and Smereka, 1997) demonstrating the splitting of the bubble into two. The dimensionless parameters described in (Ding *et al.*, 2007) are converted to dimensional form following which the simulation variables considered are as follows,  $R = 0.25m$ ,  $g = 9.81m.s^{-2}$ ,  $\rho_1 = 1.0 kg.m^{-3}$ ,  $\rho_2 = 1000 kg.m^{-3}$ ,  $\mu_1 = 3.915 Pa.s$ ,  $\mu_2 = 0.03915 Pa.s$  and  $\sigma = 3.065 N.m^{-1}$ .

Herein, the values of viscosity and surface tension are obtained from the corresponding Reynolds and Bond numbers of 100 and 200, respectively as in (Ding *et al.*, 2007) while the domain size is given by ( $L = 4R, H = 8R$ ). We compare here the  $y$  –position at which the bubble is about to split and is given by  $4.05 R = 1.0125 m$  as described in (Ding *et al.*, 2007) which in the present case is found to be at  $y = 1.02 m$  ( an error of 0.75 % is found). As before, we further compare the results obtained using AITM-PFM and LSM and a close match is observed as shown in **Error! Reference source not found.**

The observed splitting up of the bubble resulting in toroidal shape is in coherence with that described in the literature (Tripathi *et al.*, 2015) for the chosen parameters (Reynolds number = 100 and Bond number = 200). While a detailed discussion can be found elsewhere (Bonometti and Magnaudet, 2006; Chen *et al.*, 1999), we provide a brief overview of the observed behavior. At the start of the bubble rise, the presence of a higher-pressure gradient at the bottom of the bubble as compared due to the top one makes the fluid to move in at the bottom surface. This stream of fluid, which can be considered as a jet, pushes further into the lower surface eventually piercing the top surface resulting in the splitting of the bubble as observed in **Error! Reference source not found.** It is worth mentioning that for a higher surface tension, a higher resistance to the piercing of the upper surface will be present thereby leading to a different terminal shape. A more detailed discussion on these can be found in the aforementioned references.

#### 7.4 Coalescence of bubbles.

As a final test case we consider the problem of the coalescence of two bubbles in a close proximity of each other (schematic shown in **Error! Reference source not found.**,  $\rho_1 = \rho_2 = 1000 \text{ kg.m}^{-3}$ ,  $\mu_1 = \mu_2 = 0.1 \text{ Pa.s}$  and  $\sigma = 1 \text{ N.m}^{-1}$ ) to form a single unit. While the physical phenomenon causing this can be found in (Aarts *et al.*, 2005), our objective lies in capturing this behavior from numerical perspectives. It is expected that the bubbles will approach each other and once the coalescence begins, their shape will become an ellipse with major axis oscillating from  $y$  to  $x$  before finally settling to a circular shaped bubble. One of the major issues addressed in the context of this problem with incorrect mobility is that it leads to bubble entrapment (Magaletti *et al.*, 2013) which is not physical in nature. For the sake of illustration, we run a simulation with constant  $M_o = 10^{-10}$  for which the final shape (contour plot) along with  $\phi$  profile at  $y = 0.5m$  is shown in **Error! Reference source not found.**(a) describing the aforesaid problem as has also been mentioned in (Magaletti *et al.*, 2013). When the bubbles start to coalesce, the local region at which the bubbles come in contact move to a state of disequilibrium which can be represented by sharp

gradients in  $\phi$  profile. In order to have correct coalescence, appropriate mobility should be able to diffuse these gradients fast enough so as to match the interface dynamics due to inertia. At a low value, the desired level of diffusion fails to occur causing entrapment of one phase in another as shown in **Error! Reference source not found.**(a). However, it is quite intuitive to understand that this is not what is expected in real sense and appropriate results can be attained at a higher value of mobility ( $M_o = 10^{-5}$ ) as shown in **Error! Reference source not found.**(b). It is to be noted that in case of incorrect mobility, even though we may be able to match the other behavior such as final shape or Laplace pressure jump after coalescence, the results would still be incorrect as this type of entrapment is not expected and in more complicated analysis can lead to erroneous results.

We now use our approach to demonstrate the evolution of the bubble which is shown at various time instances in **Error! Reference source not found.**. It can be seen that bubbles coalesce to form a circular shape while no entrapment is observed, following the same intermittent shapes as in (Magaletti *et al.*, 2013), owing to local mobility being adapted to ensure equilibrium is attained in coherence with time scale of the physical dynamics. This is further evident from **Error! Reference source not found.** wherein  $\phi$  profile along  $x$  axis is drawn at  $y = 0.5 m$  at various time instances. It is clear that the shape of the bubbles oscillates initially and thus so does the  $\phi$  profile before settling to a smooth  $\tanh$  type profile as is clear in **Error! Reference source not found.**(c).

## 8. Conclusion

The current work presents a new approach to obtain an appropriate value of mobility based on the local interface thickness. Starting with the description of the classical phase-field model as presented in the literature, we validate our numerical methodology, primarily for the phase-field equation wherein we use a second-order implicit central differencing scheme for the fourth order derivative term, using canonical test cases (droplet in equilibrium and advection of the bubble). The results also highlight the need to consider additional terms when using the potential form of surface tension term to ensure the correct pressure jump condition across the interface. Furthermore, a more stringent case of rise of a lighter fluid in a heavier medium illustrates the influence of mobility on the outcome of the solution. Herein, we address this problem using an innovative methodology defining it as adaptive interface thickness based mobility-phase field method (AITM-PFM). Assuming local equilibrium conditions, we reverse calculate the corresponding 'equilibrium' interface thickness thereby implicitly implying that each sub-volume is an independent system *w. r. t* phase field and tend to move towards equilibrium within the time scale of the

bulk phenomena. This permits to use the local velocity (magnitude) as the velocity scale in the relation of mobility, available in terms of non-dimensional numbers including characteristic velocity, and thus facilitates its straightforward utility to physical systems. The developed methodology thus helps to overcome the ambiguities in the choice of appropriate velocity scale which can eventually lead to the introduction of another numerical factor in the model thereby rendering the fidelity of the PFM dependent on numerical parameter. AITM-PFM is validated via various test cases varying from a simple bubble rise to more complicated ones involving splitting / merging of the interface. **The proposed method, in addition to solving the governing equations of PFM as described in literature, needs to evaluate just an additional relation as described by Eq. 12 whilst using a simple numerical discretization scheme when compared to the more sophisticated ones used in the literature (Badalassi *et al.*, 2003; Ding *et al.*, 2007). It can thereby be ascertained that the current method does not add to any computational losses when compared to usual PFM though the inherit limitation of PFM in terms of computational cost do come along. Nevertheless, among the two major limitations of PFM as described in §1, we have addressed the problem of appropriate choice of mobility parameter using AITM-PFM and this opens up new perspectives to use this method in conjunction with adaptive mesh or to look for other possible solutions to address the problem associated with computational costs in PFM. The method can thus be seen as a significant improvement to address the challenges in the phase-field method and expand the utility of phase-field method to more physically complex problems involving large topological changes.**

### **Acknowledgement**

This work is benefited from the support of the French Space Agency (CNES). The authors acknowledge the support from supercomputing facilities (Condor) at Lab. I2M and wish to thank Dr. Stéphane Glockner for his help with the Notus code (<https://notus-cfd.org/>).

## References

- A Mirjalili, B.S., A Jain, S.S., A Dodd, M.S., Interface-capturing methods for two-phase flows : An overview and recent developments, in: 2017 (Ed.), Center for Turbulence Research Annual Research Briefs.
- Aarts, D.G.A.L., Lekkerkerker, H.N.W., Guo, H., Wegdam, G.H., Bonn, D., 2005. Hydrodynamics of Droplet Coalescence. *Physical Review Letters* 95, 164503.
- Abels, H., Garcke, H., Grun, G., 2012. Thermodynamically consistent, frame indifferent diffuse interface models for incompressible two-phase flows with different densities. *Mathematical Models and Methods in Applied Sciences* 22, 1150013.
- Aland, S., Voigt, A., 2012. Benchmark computations of diffuse interface models for two-dimensional bubble dynamics. *International Journal for Numerical Methods in Fluids* 69, 747-761.
- Allen, S.M., Cahn, J.W., 1972. Ground state structures in ordered binary alloys with second neighbor interactions. *Acta Metallurgica* 20, 423-433.
- Allen, S.M., Cahn, J.W., 1973. A correction to the ground state of FCC binary ordered alloys with first and second neighbor pairwise interactions. *Scripta Metallurgica* 7, 1261-1264.
- Anderson, D.M., McFadden, G.B., Wheeler, A.A., 1998. Diffuse-interface methods in fluid mechanics. *Annual Review of Fluid Mechanics* 30, 139-165.
- Antanovskii, L.K., 1995. A phase field model of capillarity. *Physics of Fluids* 7, 747-753.
- Asuri Mukundan, A., Ménard, T., Brändle de Motta, J.C., Berlemont, A., 2020. A 3D Moment of Fluid method for simulating complex turbulent multiphase flows. *Computers & Fluids* 198, 104364.
- Badalassi, V.E., Cenicerros, H.D., Banerjee, S., 2003. Computation of multiphase systems with phase field models. *Journal of Computational Physics* 190, 371-397.
- Bonometti, T., Magnaudet, J., 2006. Transition from spherical cap to toroidal bubbles. *Physics of Fluids* 18, 052102.
- Borcia, R., Borcia, I.D., Bestehorn, M., 2008. Drops on an arbitrarily wetting substrate: A phase field description. *Physical Review E* 78, 066307.
- Borcia, R., Borcia, I.D., Bestehorn, M., 2014. Can Vibrations Control Drop Motion? *Langmuir* 30, 14113-14117.
- Boyer, F., 2002. A theoretical and numerical model for the study of incompressible mixture flows. *Computers & Fluids* 31, 41-68.
- Cahn, J.W., Hilliard, J.E., 1958. Free Energy of a Nonuniform System. I. Interfacial Free Energy. *The Journal of Chemical Physics* 28, 258-267.
- Cahn, J.W., Hilliard, J.E., 1959. Free Energy of a Nonuniform System. III. Nucleation in a Two-Component Incompressible Fluid. *The Journal of Chemical Physics* 31, 688-699.

Chen, L.I., Garimella, S.V., Reizes, J.A., Leonardi, E., 1999. The development of a bubble rising in a viscous liquid. *Journal of Fluid Mechanics* 387, 61-96.

Chorin, A.J., 1967. A numerical method for solving incompressible viscous flow problems. *Journal of Computational Physics* 2, 12-26.

Coquerelle, M., Glockner, S., 2016. A fourth-order accurate curvature computation in a level set framework for two-phase flows subjected to surface tension forces. *Journal of Computational Physics* 305, 838-876.

Desmons, F., Coquerelle, M., 2020. A generalized high-order momentum preserving (HOMP) method in the one-fluid model for incompressible two phase flows with high density ratio.

Ding, H., Spelt, P.D.M., Shu, C., 2007. Diffuse interface model for incompressible two-phase flows with large density ratios. *Journal of Computational Physics* 226, 2078-2095.

Emmerich, H., 2008. Advances of and by phase-field modelling in condensed-matter physics. *Advances in Physics* 57, 1-87.

Gibou, F., Fedkiw, R., Osher, S., 2018. A review of level-set methods and some recent applications. *Journal of Computational Physics* 353, 82-109.

Guo, Z., Lin, P., 2015. A thermodynamically consistent phase-field model for two-phase flows with thermocapillary effects. *Journal of Fluid Mechanics* 766, 226-271.

Gurtin, M.E., Polignone, D., ViÑAls, J., 1996. Two-phase binary fluids and immiscible fluids described by an order parameter. *Mathematical Models and Methods in Applied Sciences* 06, 815-831.

Haghshenas, M., Wilson, J.A., Kumar, R., 2017. Algebraic coupled level set-volume of fluid method for surface tension dominant two-phase flows. *International Journal of Multiphase Flow* 90, 13-28.

Helmut Abels, Harald Garacke, Günther Grün, Metzger, S., 2017. *Transport Processes at Fluidic Interfaces*. Birkhäuser Basel.

Hohenberg, P.C., Halperin, B.I., 1977. Theory of dynamic critical phenomena. *Reviews of Modern Physics* 49, 435-479.

Hong, J.-M., Shinar, T., Kang, M., Fedkiw, R., 2007. On Boundary Condition Capturing for Multiphase Interfaces. *Journal of Scientific Computing* 31, 99-125.

Hou, T.Y., Lowengrub, J.S., Shelley, M.J., 1997. The long-time motion of vortex sheets with surface tension. *Physics of Fluids* 9, 1933-1954.

Hou, T.Y., Lowengrub, J.S., Shelley, M.J., 2001. Boundary Integral Methods for Multicomponent Fluids and Multiphase Materials. *Journal of Computational Physics* 169, 302-362.

Hua, J., Lin, P., Liu, C., Wang, Q., 2011. Energy law preserving CO finite element schemes for phase field models in two-phase flow computations. *Journal of Computational Physics* 230, 7115-7131.

- Hysing, S., Turek, S., Kuzmin, D., Parolini, N., Burman, E., Ganesan, S., Tobiska, L., 2009. Quantitative benchmark computations of two-dimensional bubble dynamics. *International Journal for Numerical Methods in Fluids* 60, 1259-1288.
- Jacqmin, D., 1999. Calculation of Two-Phase Navier–Stokes Flows Using Phase-Field Modeling. *Journal of Computational Physics* 155, 96-127.
- Jost, A.M.D., Glockner, S., Erriguible, A., 2020. Direct numerical simulations of fluids mixing above mixture critical point. *The Journal of Supercritical Fluids* 165, 104939.
- Kajzer, A., Pozorski, J., 2020. A weakly Compressible, Diffuse-Interface Model for Two-Phase Flows. *Flow, Turbulence and Combustion* 105, 299-333.
- Kim, J., 2015. Phase-Field Models for Multi-Component Fluid Flows. *Communications in Computational Physics* 12, 613-661.
- Lowengrub, J., Truskinovsky, L., 1998. Quasi-incompressible Cahn–Hilliard fluids and topological transitions. *Proceedings of the Royal Society of London. Series A: Mathematical, Physical and Engineering Sciences* 454, 2617.
- Magaletti, F., Picano, F., Chinappi, M., Marino, L., Casciola, C.M., 2013. The sharp-interface limit of the Cahn–Hilliard/Navier–Stokes model for binary fluids. *Journal of Fluid Mechanics* 714, 95-126.
- Milcent, T., Lemoine, A., 2020. Moment-of-fluid analytic reconstruction on 3D rectangular hexahedrons. *Journal of Computational Physics* 409, 109346.
- Mirjalili, S., Ivey, C.B., Mani, A., 2019. Comparison between the diffuse interface and volume of fluid methods for simulating two-phase flows. *International Journal of Multiphase Flow* 116, 221-238.
- Mirjalili, S., Ivey, C.B., Mani, A., 2020. A conservative diffuse interface method for two-phase flows with provable boundedness properties. *Journal of Computational Physics* 401, 109006.
- Olsson, E., Kreiss, G., Zahedi, S., 2007. A conservative level set method for two phase flow II. *Journal of Computational Physics* 225, 785-807.
- Osher, S., Sethian, J.A., 1988. Fronts propagating with curvature-dependent speed: Algorithms based on Hamilton-Jacobi formulations. *Journal of Computational Physics* 79, 12-49.
- Rowlinson, J.S., 1979. Translation of J. D. van der Waals' "The thermodynamik theory of capillarity under the hypothesis of a continuous variation of density". *Journal of Statistical Physics* 20, 197-200.
- Shen, J., Yang, X., 2010. A Phase-Field Model and Its Numerical Approximation for Two-Phase Incompressible Flows with Different Densities and Viscosities. *SIAM Journal on Scientific Computing* 32, 1159-1179.
- Sibley, D.N., Nold, A., Kalliadasis, S., 2013. Unifying binary fluid diffuse-interface models in the sharp-interface limit. *Journal of Fluid Mechanics* 736, 5-43.

Sussman, M., 2003. A second order coupled level set and volume-of-fluid method for computing growth and collapse of vapor bubbles. *Journal of Computational Physics* 187, 110-136.

Sussman, M., Puckett, E.G., 2000. A Coupled Level Set and Volume-of-Fluid Method for Computing 3D and Axisymmetric Incompressible Two-Phase Flows. *Journal of Computational Physics* 162, 301-337.

Sussman, M., Smereka, P., 1997. Axisymmetric free boundary problems. *Journal of Fluid Mechanics* 341, 269-294.

Takagi, K., Matsumoto, T., 2011. Numerical simulation of two-dimensional Faraday waves with phase-field modelling. *Journal of Fluid Mechanics* 686, 409-425.

Tripathi, M.K., Sahu, K.C., Govindarajan, R., 2015. Dynamics of an initially spherical bubble rising in quiescent liquid. *Nature Communications* 6, 6268.

Tryggvason, G., Bunner, B., Esmaeeli, A., Juric, D., Al-Rawahi, N., Tauber, W., Han, J., Nas, S., Jan, Y.J., 2001. A Front-Tracking Method for the Computations of Multiphase Flow. *Journal of Computational Physics* 169, 708-759.

Wang, R., Spiteri, R.J., 2007. Linear Instability of the Fifth-Order WENO Method. *SIAM Journal on Numerical Analysis* 45, 1871-1901.

Wang, Y., Cai, J., Li, Q., Yin, H., Yang, X., 2018. Diffuse interface simulation of bubble rising process: a comparison of adaptive mesh refinement and arbitrary lagrange-euler methods. *Heat and Mass Transfer* 54, 1767-1778.

Xu, X., Di, Y., Yu, H., 2018. Sharp-interface limits of a phase-field model with a generalized Navier slip boundary condition for moving contact lines. *Journal of Fluid Mechanics* 849, 805-833.

Yue, P., Zhou, C., Feng, J.J., 2010. Sharp-interface limit of the Cahn–Hilliard model for moving contact lines. *Journal of Fluid Mechanics* 645, 279-294.

Zuzio, D., Estivaleres, J.L., 2011. An efficient block parallel AMR method for two phase interfacial flow simulations. *Computers & Fluids* 44, 339-357.

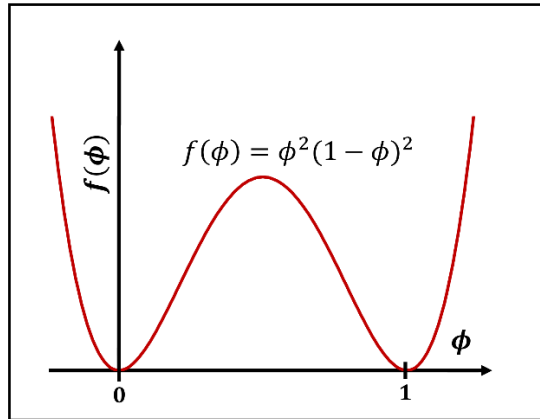


Figure 1: Schematic of double well polynomial representing the bulk free energy function .

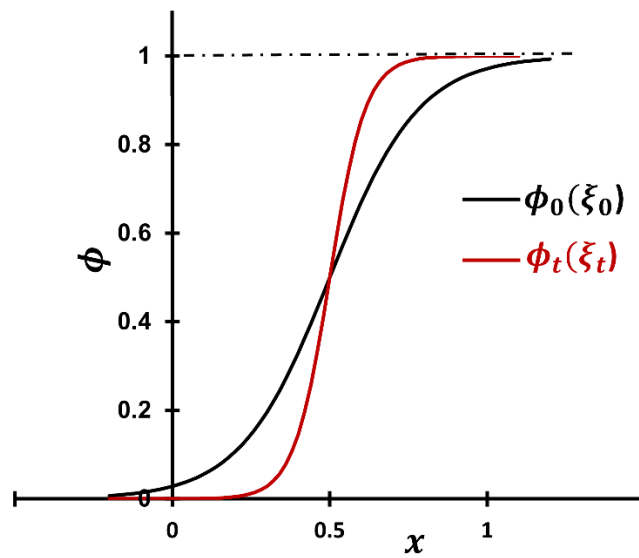


Figure 2: Schematic of interface profile illustrating shrinkage of interface thickness w.r.t  $\xi_0$ .

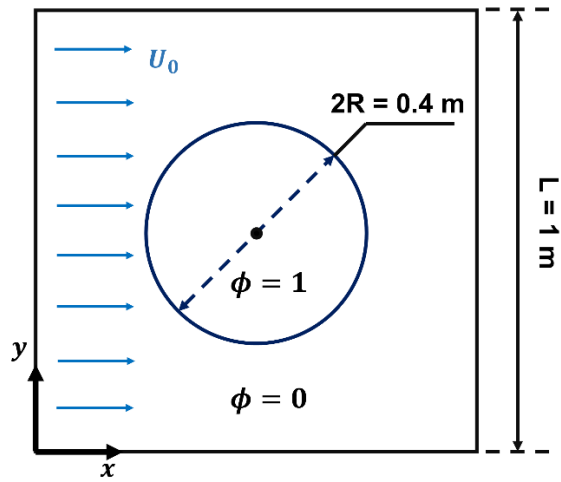


Figure 3: Schematic of test case for droplet in equilibrium ( $U_0 = 0 \text{ m/s}$ ) and advection of drop in  $x$  direction with different  $U_0 > 0$  as in §6.2.

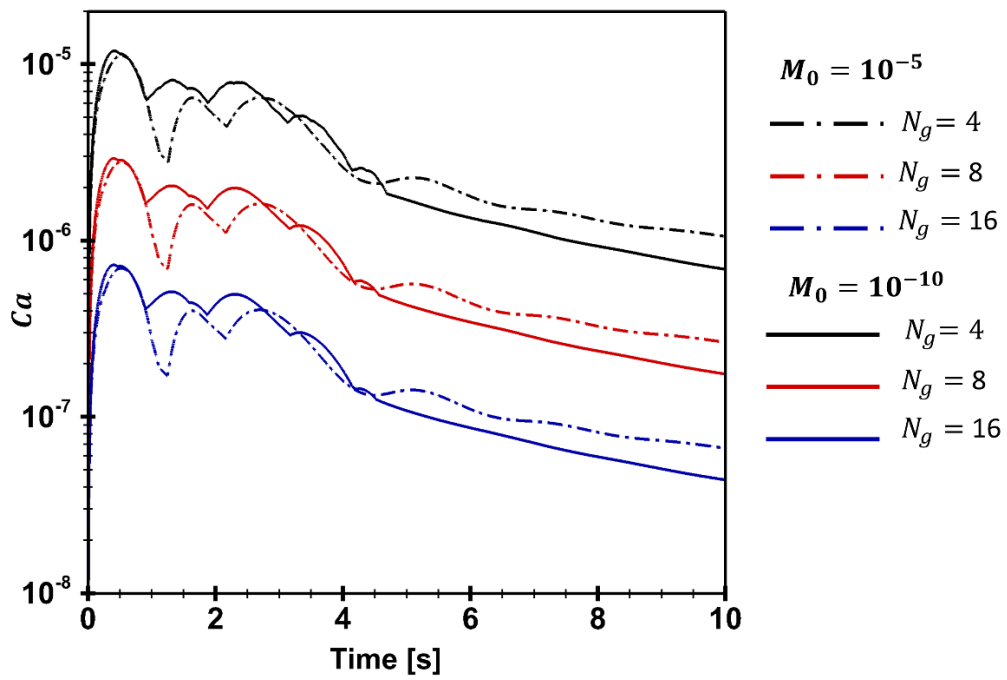


Figure 4: Evolution of  $Ca$  for the case of droplet in equilibrium ( $U_0 = 0 \text{ m/s}$ ) for  $Cn = 0.1$  on a semi-log plot.

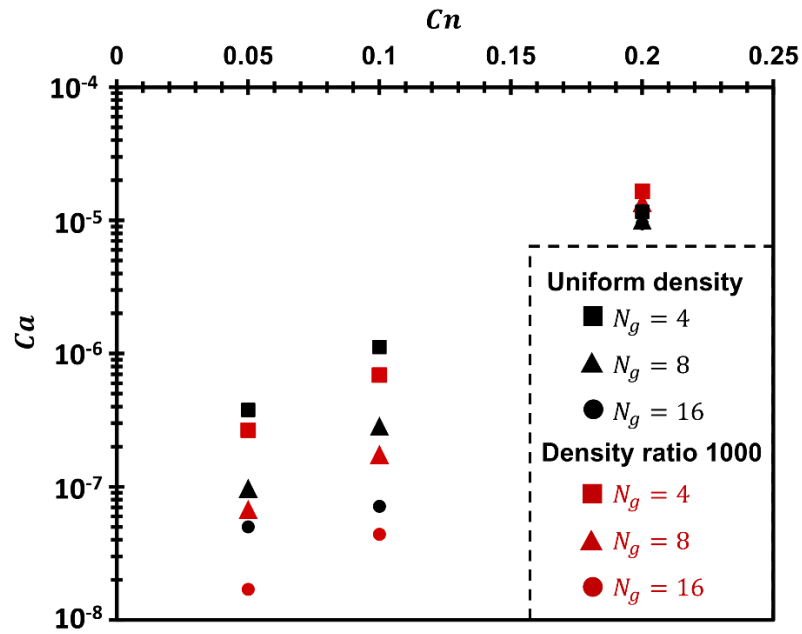


Figure 5: Variation of  $Ca$  for different  $Cn$  at  $t^* = 250$  for uniform density and density ratio of 1000.

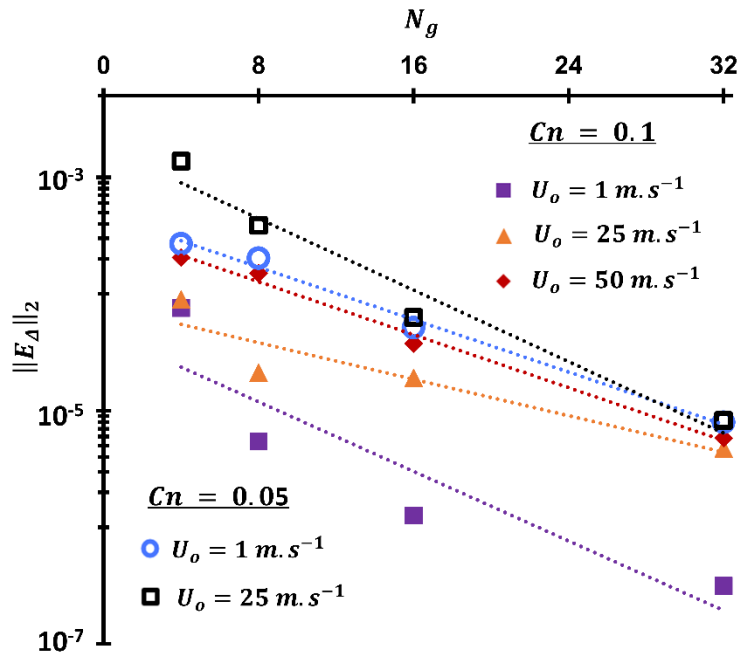


Figure 6:  $\|E_\Delta\|_2$  for different advection velocities for system with uniform density as function of number of grid points in the interface for  $Cn = 0.1$  and  $0.05$ .

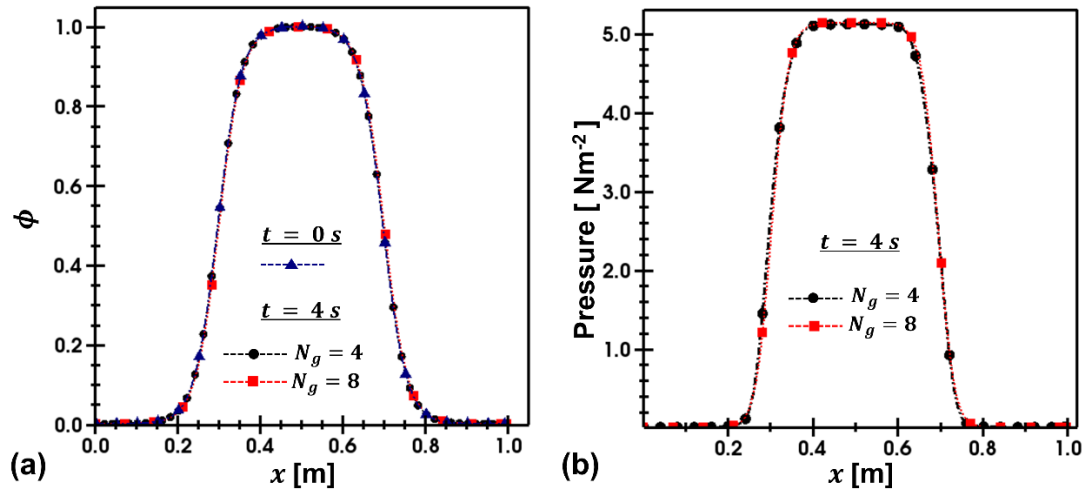


Figure 7: (a) Phase field  $\phi$  and (b) pressure profiles at  $y = 0.5 \text{ m}$  and  $t = 4 \text{ s}$  for  $Cn = 0.1$ ,  $U_o = 1 \text{ ms}^{-1}$  for different  $N_g$ .

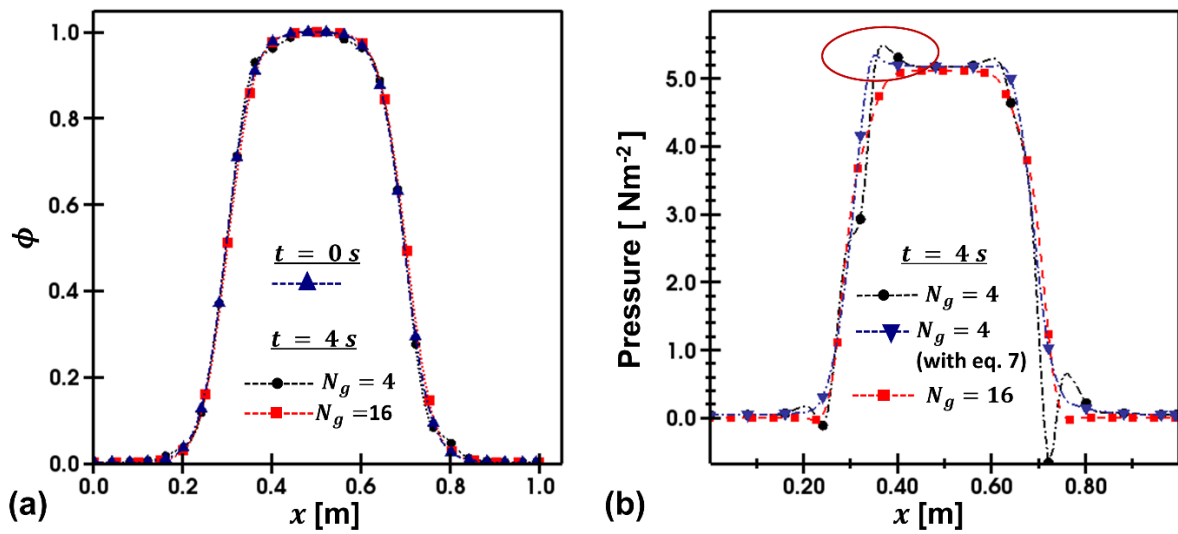


Figure 8: (a) Phase field  $\phi$  and (b) pressure profiles at  $y = 0.5 \text{ m}$  and  $t = 4 \text{ s}$  for  $Cn = 0.1$  and  $U_o = 25 \text{ m.s}^{-1}$  for different  $N_g$ . (b) the pressure profile for the model which includes terms as given in Eq. (7) by (Jacqmin, 1999) is also shown. The encircled region represents region where unphysical pressure jump is observed with this model and the one from (Jacqmin, 1999).

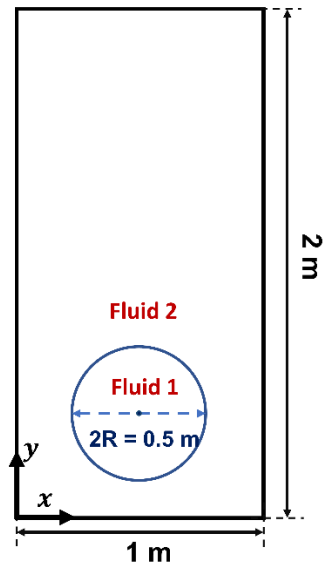


Figure 9: Schematic of the rise of a lighter bubble in a heavier medium.

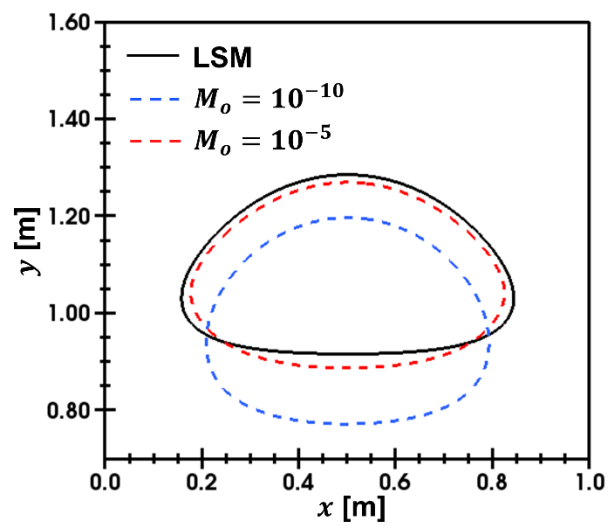


Figure 10: Position of the bubble at  $t = 3 \text{ s}$  with level set method (LSM) and phase field method (PFM) for different values of mobility.

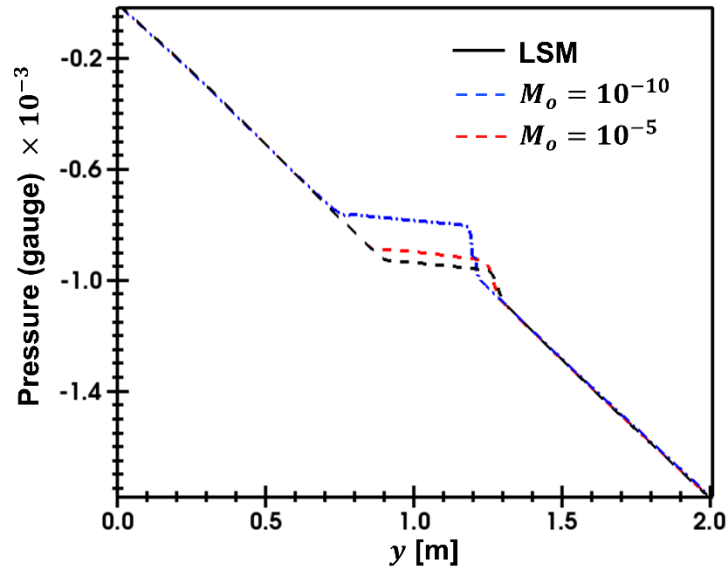


Figure 11: Pressure profile at  $x = 0.5 \text{ m}$  plane with LSM and PFM for different values of mobility.

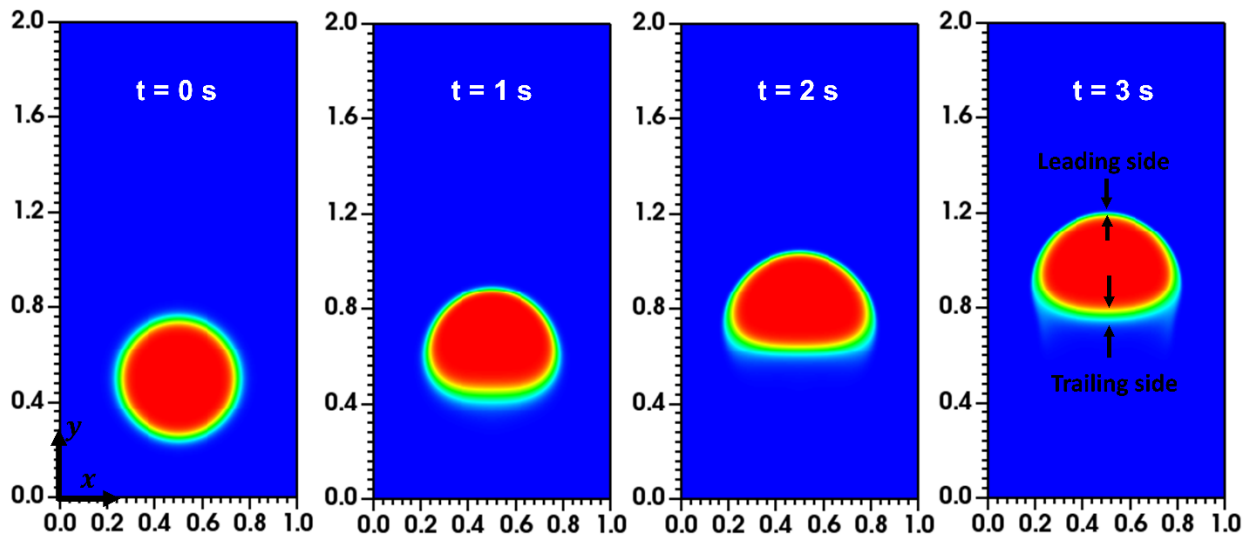


Figure 12: Position of the bubble at various time intervals with PFM for  $M_o = 10^{-10}$ . Herein  $\phi$  – field plot has been used to illustrate the position owing to its variation from 0 (red) to 1 (blue) and has been used in all the figures henceforth.

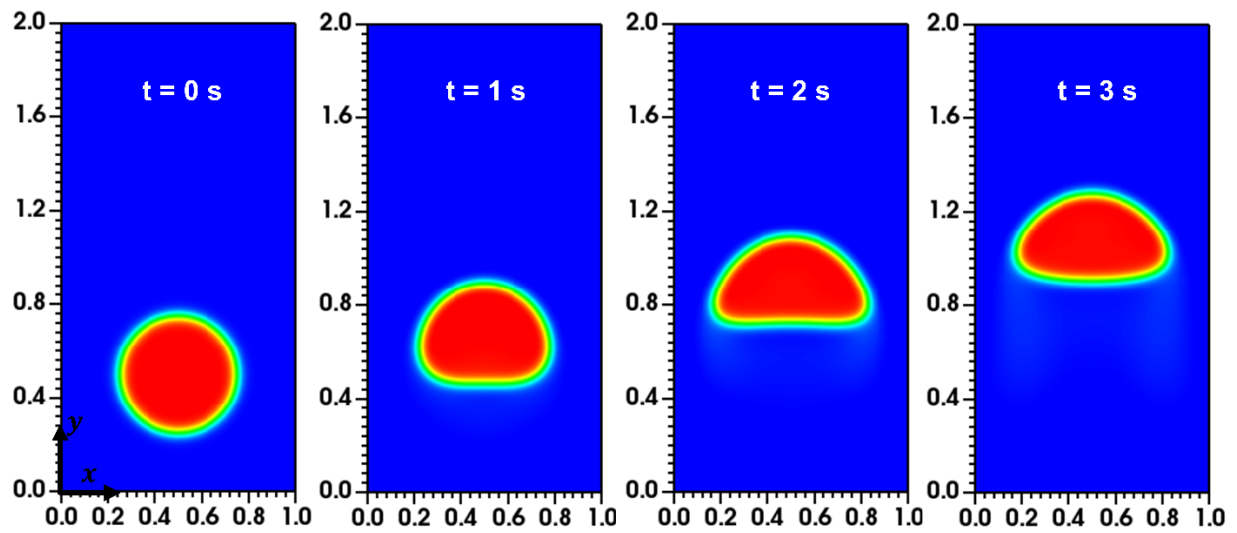


Figure 13: Position of bubble at various time intervals for  $M_o = 10^{-5}$ .

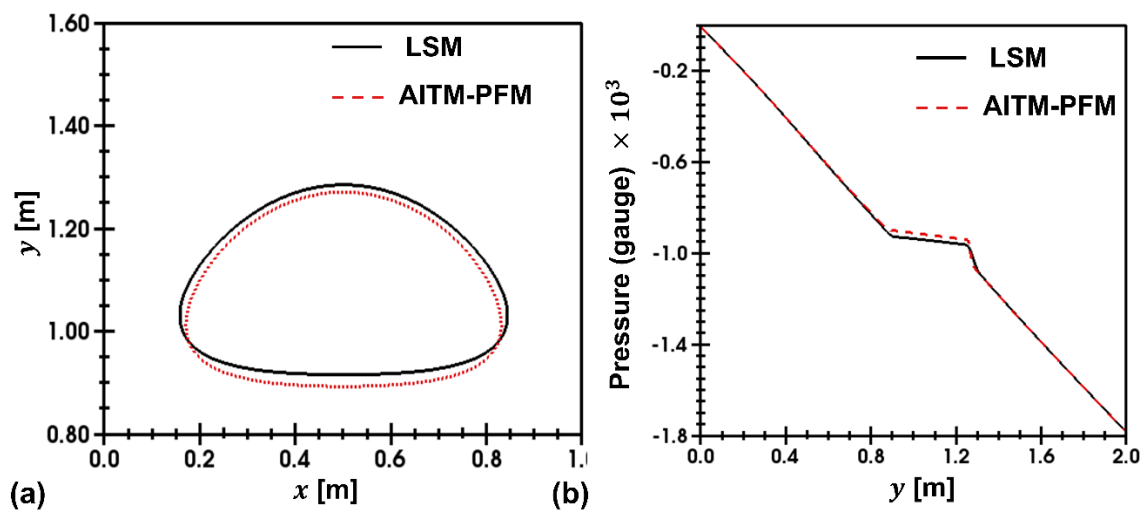


Figure 14: (a) Position of the bubble (b) pressure field at  $x = 0.5\text{ m}$  plane at  $t = 3\text{ s}$  using LSM and AITM-PFM.

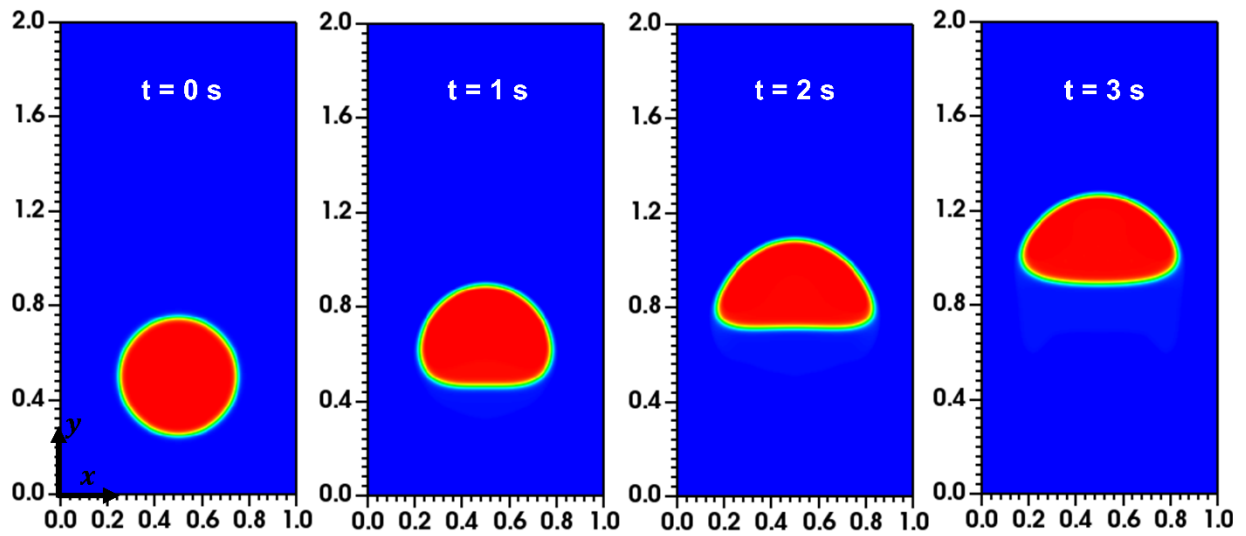


Figure 15: Position of bubble at various time intervals with AITM-PFM.

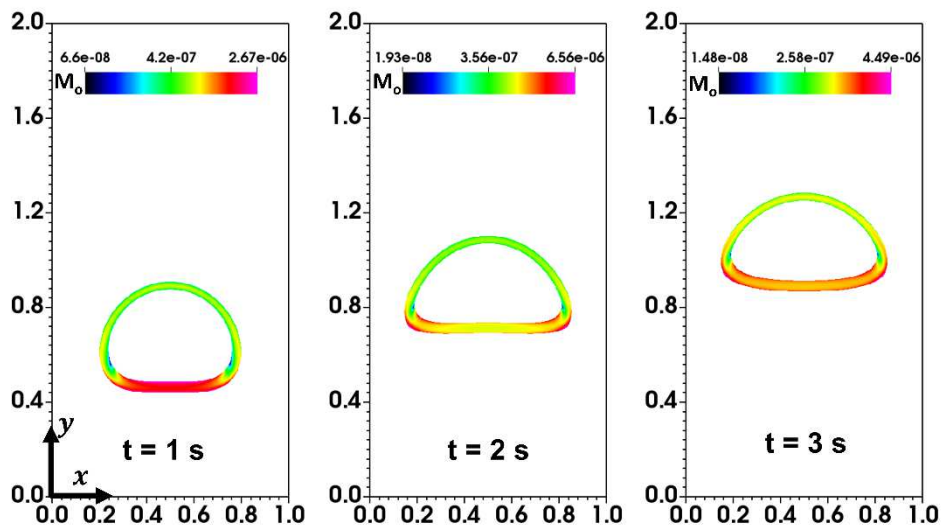


Figure 16: Evolution of  $M_0$  for the results shown in Figure 15 using the relation given in Eq. Error! Reference source not found. with local interface thickness evaluated using Eq. Error! Reference source not found..

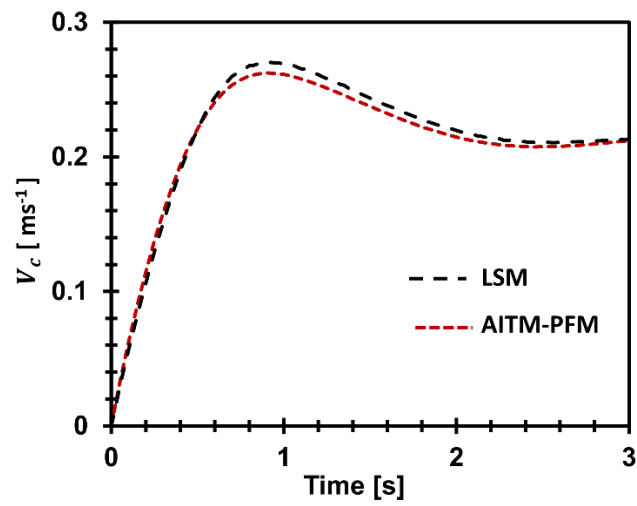


Figure 17: Average velocity of rise of bubble using LSM and AITM-PFM

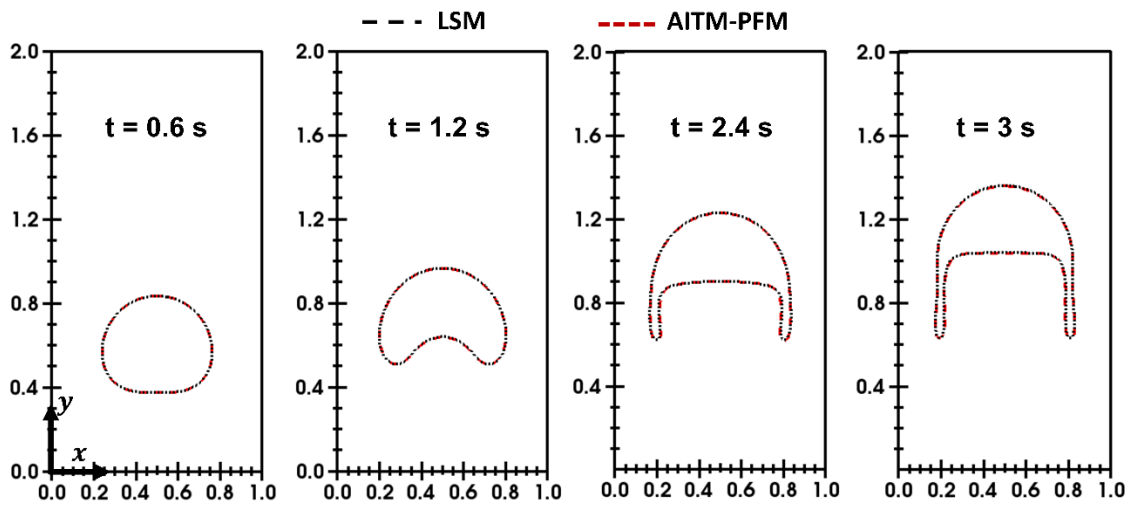


Figure 18: Position of bubble at various time instances using LSM and AITM-PFM ( $Cn = 0.02$  and  $N_g = 10$ ) (case: density ratio 1000).

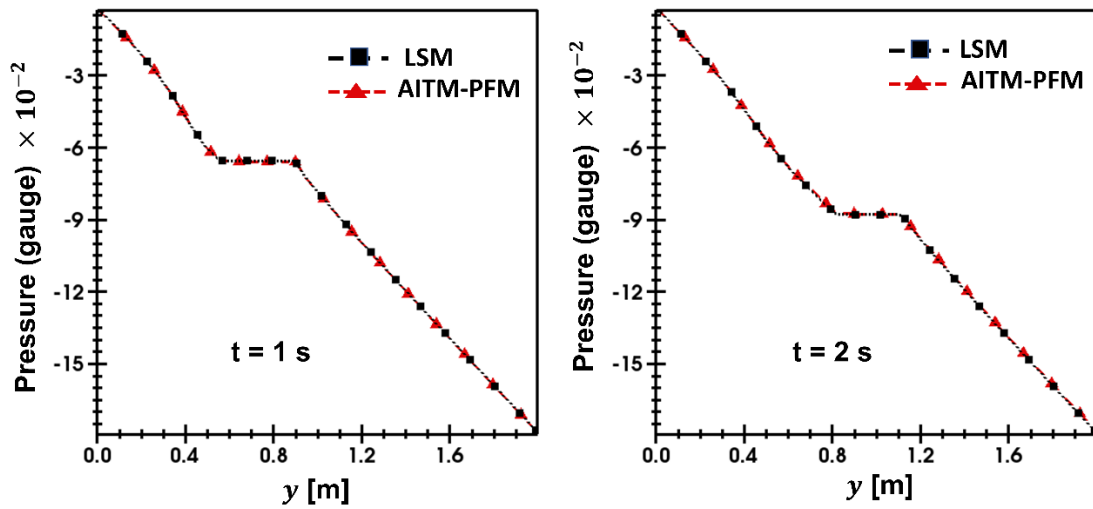


Figure 19: Pressure profile at  $x = 0.5$  m plane at  $t = 1$  s and  $t = 2$  s using LSM and AITM-PFM (case: density ratio 1000).

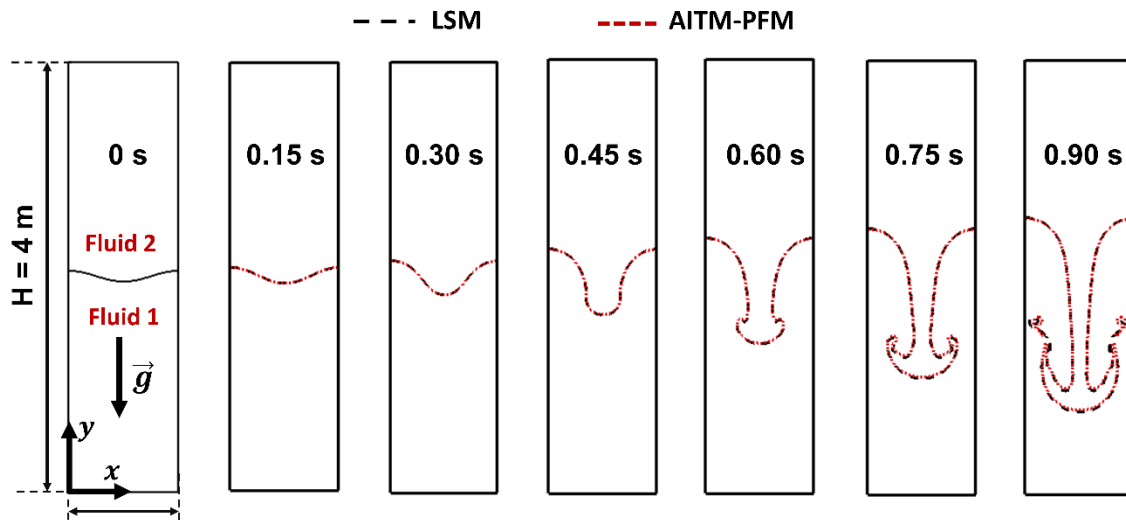


Figure 20: Comparison of the interface position in case of Rayleigh Taylor instability at various time steps using AITM-PFM and LSM.

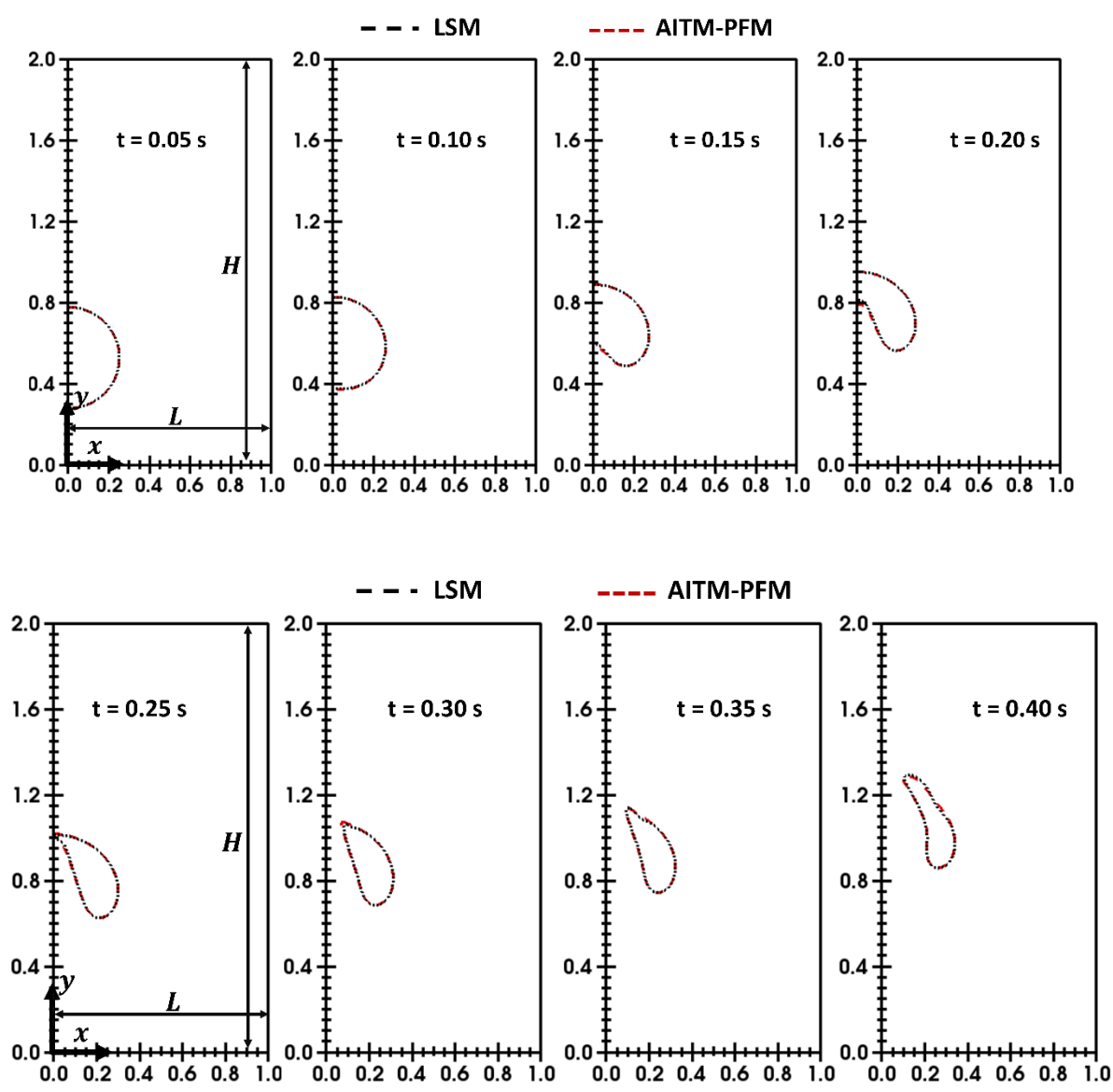


Figure 21 Position of bubble at various time instances using AITM-PFM and LSM.

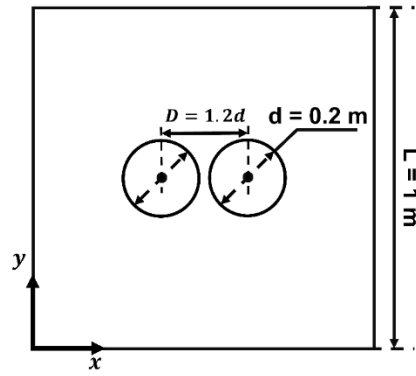


Figure 22: Schematic of bubble coalescence.

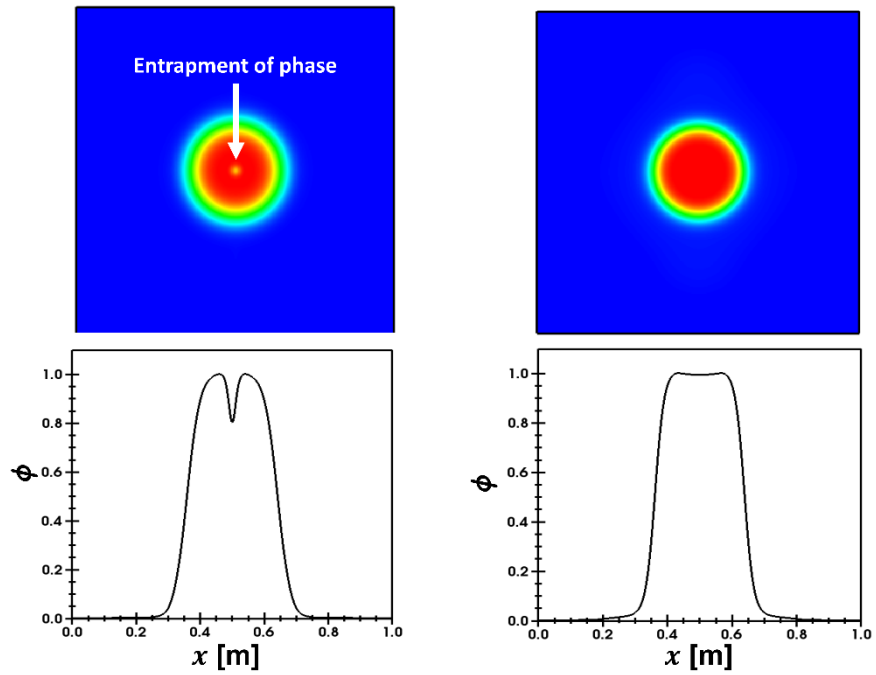


Figure 23 Coalescence of bubbles with constant interface thickness and thus mobility (a)  $M_o = 10^{-10}$  (b)  $M_o = 10^{-5}$ .

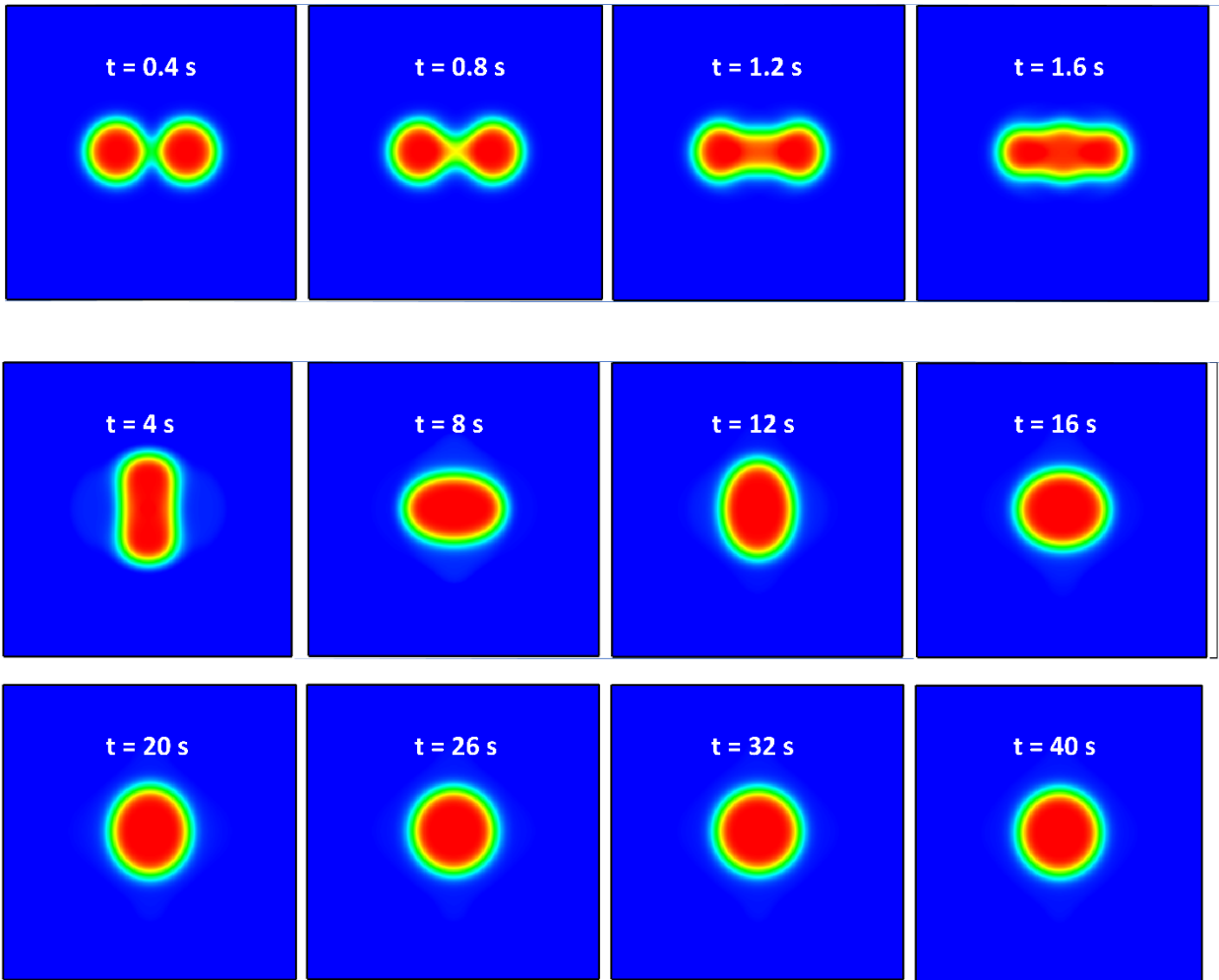


Figure 24 Coalescence to bubbles at various time intervals using AITM-PFM.

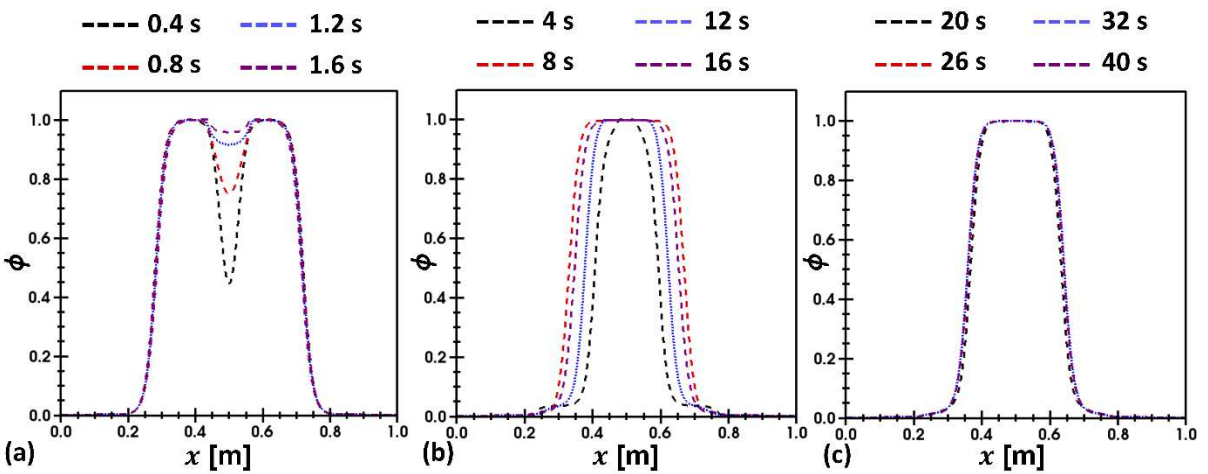


Figure 25  $\phi$  –profile along  $x$  axis at  $y = 0.5 \text{ m}$  for time instances illustrated in Figure 24.